Cell Reports

Article

Pharmacological administration of FGF21 reverses obesity through a parabrachial-projecting neuron population in the hindbrain

Graphical abstract

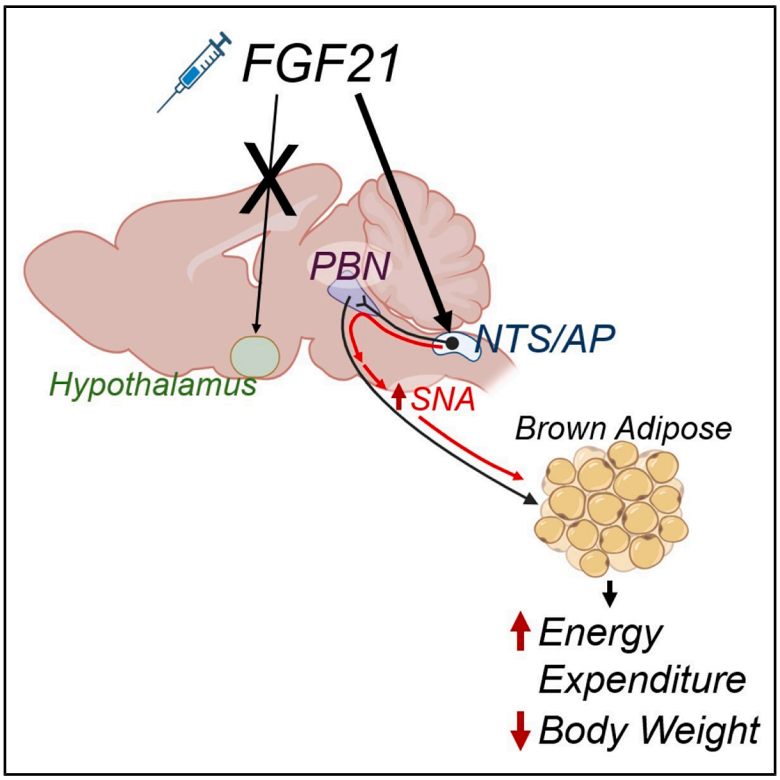

Authors

Yunfan Lin, Kristin E. Claflin, Iltan Aklan, ..., Michael C. Rudolph, Kamal Rahmouni, Matthew J. Potthoff

Correspondence

matthew-potthoff@ou.edu

In brief

Lin et al. reveal that FGF21 acts on the hindbrain (nucleus of the solitary tract [NTS] and area postrema [AP]), and not the hypothalamus, to reduce body weight. Specifically, FGF21 signaling to the hindbrain activates local KLB^{+} Vglut2^{+} neurons that project to the parabrachial nucleus to promote energy expenditure.

Highlights

- FGF21 signaling in the hypothalamus is not required to reduce body weight
- FGF21 signaling in the hindbrain (NTS/AP) is required to drive weight loss
- FGF21 action in the hindbrain is sufficient to activate BAT thermogenesis
- FGF21 signals to KLB$^{NTS/AP \rightarrow PBN}$-projecting neurons to reduce body weight

Lin et al., 2026, Cell Reports *45*, 117093
April 28, 2026 Published by Elsevier Inc.
https://doi.org/10.1016/j.celrep.2026.117093

CellPress

Cell Reports

CellPress
OPEN ACCESS

Article

Pharmacological administration of FGF21 reverses obesity through a parabrachial-projecting neuron population in the hindbrain

Yunfan Lin,[1,2,3,6,7,8] Kristin E. Claflin,[1,2,3,8] Iltan Aklan,[6,7,8] Donald A. Morgan,[1] Andrew I. Sullivan,[1,2,3] Michael C. Rudolph,[6,7] Kamal Rahmouni,[1,2,3,4,5] and Matthew J. Potthoff[1,2,3,5,6,7,9,*]

[1]Department of Neuroscience and Pharmacology, University of Iowa Carver College of Medicine, Iowa City, IA 52242, USA
[2]Fraternal Order of Eagles Diabetes Research Center, University of Iowa Carver College of Medicine, Iowa City, IA 52242, USA
[3]Iowa Neuroscience Institute, University of Iowa Carver College of Medicine, Iowa City, IA 52242, USA
[4]Department of Internal Medicine, University of Iowa Carver College of Medicine, Iowa City, IA 52242, USA
[5]Iowa City VA Health Care System, Iowa City, IA 52242, USA
[6]Harold Hamm Diabetes Center, University of Oklahoma Health Sciences, Oklahoma City, OK 73104, USA
[7]Department of Biochemistry and Physiology, University of Oklahoma Health Sciences, Oklahoma City, OK 73104, USA
[8]These authors contributed equally
[9]Lead contact
*Correspondence: matthew-potthoff@ou.edu
https://doi.org/10.1016/j.celrep.2026.117093

SUMMARY

The obesity epidemic is associated with significant healthcare and economic burdens. Pharmacological administration of the endocrine hormone fibroblast growth factor 21 (FGF21) increases energy expenditure and reverses obesity. However, the central targets and neural pathways for these metabolic benefits remain elusive. Here, we demonstrate that β-klotho (KLB)-expressing neurons in the hindbrain, specifically the nucleus of the solitary tract (NTS) and area postrema (AP), are both necessary and sufficient for FGF21's effect on energy expenditure and weight loss. These pharmacological benefits are mediated largely by NTS/AP KLB-expressing neurons that project to the parabrachial nucleus (PBN) and not the hypothalamus. Our results provide insights into the central mechanisms of pharmacological FGF21 action to modulate energy homeostasis.

INTRODUCTION

Obesity is a chronic, multifactorial disease caused by an imbalance between energy intake and expenditure.[1] Obesity leads to various complications, including type 2 diabetes, cardiovascular disease,[2] and cancer[3] that reduce life expectancy[4] and place a heavy burden on the healthcare system and economy.[5] Recent advances in obesity therapeutics, such as glucagon-like peptide (GLP)-1 analogs, have led to clinically meaningful weight loss by reducing calorie intake.[6,7] However, the degree of weight loss varies greatly among individuals, and patients often discontinue use due to gastrointestinal side effects.[8–10] Discontinuation of these obesity therapeutics leads to rapid weight regain, likely due to a compensatory reduction in energy expenditure.[6,8,11–13]

Fibroblast growth factor 21 (FGF21) is a predominantly liver-derived hormone that regulates energy homeostasis and macronutrient preference.[14] FGF21 signals to target tissues that express the FGF receptor 1c (FGFR1c) and the obligate co-receptor β-klotho (KLB).[15–17] KLB expression is restricted to metabolic tissues and is absolutely required for FGF21 signaling.[15–18] Pharmacological FGF21 administration significantly reduces body weight and improves lipid profiles in diet-induced obese (DIO) mice, non-human primates, and patients with obesity.[19–25] FGF21-mediated weight loss is largely attributed to an increase in energy expenditure in DIO rodents.[19,21] Physiologically, this increase in energy expenditure by FGF21 is important for brown fat thermogenesis during neonatal milk consumption,[26] and in adults for mediating the protein-leverage effect during macronutrient consumption.[27,28] However, the underlying mechanisms remain insufficiently defined. Previous studies have shown that FGF21 acts primarily on the central nervous system (CNS) to increase energy expenditure and sympathetic outflow to brown adipose tissue (BAT).[29,30] Specifically, this occurs through FGF21 signaling to glutamatergic, but not GABAergic neurons.[29] However, despite the identification of KLB-expressing glutamatergic neurons in multiple brain areas implicated in energy homeostasis, such as the hypothalamus and hindbrain, the brain region where FGF21 acts to promote energy expenditure and weight loss has not been identified.[29] In addition, although FGF21 acts on the ventromedial hypothalamus (VMH) to lower sucrose intake, FGF21 signaling to VMH KLB-expressing neurons is not required to mediate FGF21's effect on energy expenditure and body weight.[31]

The nucleus of the solitary tract (NTS) and area postrema (AP) in the hindbrain integrate central and peripheral signals to regulate energy homeostasis.[32,33] Indeed, multiple NTS/AP neuron

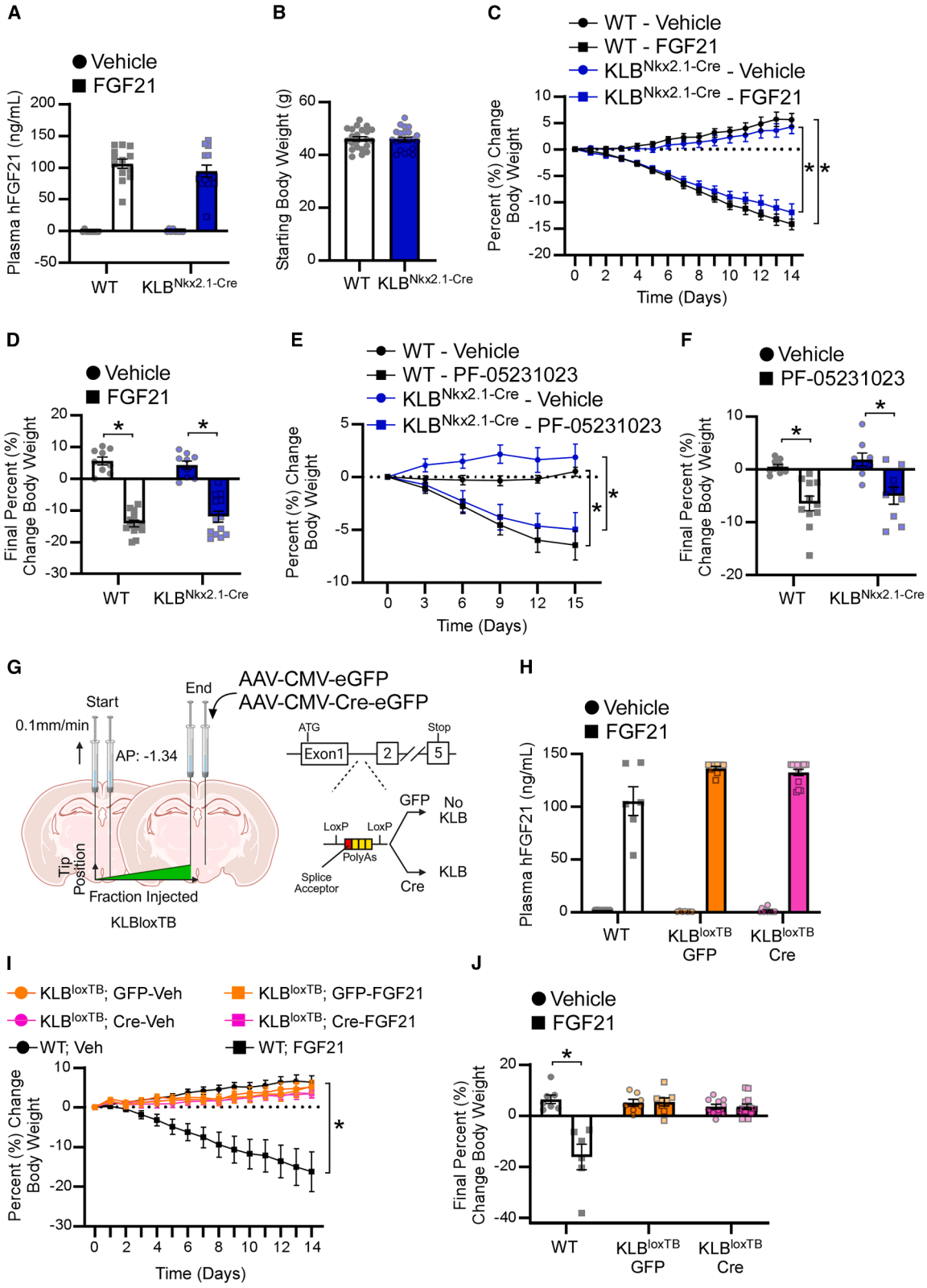

(legend on next page)

populations suppress feeding and promote negative energy balance[34–37] and are targets of several anorectic molecules, like the GLP-1 receptor agonists.[38,39] Moreover, NTS neurons connect to brain areas that regulate energy expenditure[40] and have been proposed to regulate BAT thermogenesis.[41,42] Here, we demonstrate that FGF21 signaling to neurons in the NTS/AP, but not the hypothalamus, is both necessary and sufficient for activating energy expenditure and decreasing body weight. In addition, the body weight and thermogenic effect of FGF21 in the NTS/AP are primarily mediated by neurons that project to the parabrachial nucleus (PBN). Together, this work reveals a projection-defined subset of NTS/AP neurons utilized by FGF21 to regulate energy expenditure and weight loss.

RESULTS

Pharmacological FGF21 signaling to the hypothalamus is not required or sufficient to reduce body weight

The hypothalamus is widely implicated in body weight regulation by controlling appetite and energy expenditure.[43,44] We previously identified that glutamatergic (Vglut2$^+$) KLB$^+$ neurons regulate FGF21's effects to reduce body weight, and that these Vglut2$^+$ KLB$^+$ neurons are present in metabolically relevant hypothalamic nuclei, including the paraventricular nucleus (PVN) of the hypothalamus, VMH, lateral hypothalamus (LH), dorsomedial hypothalamus (DMH), and ventral premammillary nucleus (PMv).[29] To investigate whether FGF21 signaling in the hypothalamus is required for its effect to reduce body weight, we generated mice that lack KLB in cells that have expressed NK2 homeobox 1 (Nkx2.1), a transcription factor with broad expression in the hypothalamus, by crossing Nkx2.1-Cre mice[45] with KLB$^{fl/fl}$ mice (KLB$^{Nkx2.1\text{-}Cre}$ mice). A similar approach was used previously to explore the role of the leptin receptor (LepR) in the hypothalamus.[46] The distribution of Nkx2.1 throughout the entire hypothalamus was assessed with whole organ clearing of brains harvested from Nkx2.1-Cre;Ai14-tdTomato mice using an enhanced DISCO protocol,[47] which allows visualization of tdTomato-expressing cells (Nkx2.1$^+$) across the entire brain using a light sheet fluorescence microscope. Consistent with previous characterizations of Nkx2.1-Cre mice, Nkx2.1$^+$ cells were broadly distributed in the hypothalamic regions, including but not limited to the PVN, VMH, DMH, and PMv (Video S1).[45,48,49] Importantly, Nkx2.1$^+$ cells were not expressed in the hindbrain regions, including the NTS/AP (Figure S1A).

Following chronic consumption of an obesogenic 60% high-fat diet, DIO KLB$^{Nkx2.1-Cre}$ and control DIO wild-type (WT) littermates were administered FGF21 via osmotic minipump for 14 days (Figure 1A). The starting body weight was not different between DIO KLB$^{Nkx2.1\text{-}Cre}$ and WT mice (Figure 1B). Unexpectedly, both DIO WT and KLB$^{Nkx2.1-Cre}$ animals exhibited comparable weight loss in response to FGF21 administration (Figures 1C and 1D). FGF21 treatment did not result in discernible changes in home-cage food intake (Figure S1B). To extend these findings, we administered a therapeutic FGF21 analog, PF-05231023,[24] to a separate cohort of DIO WT and KLB$^{Nkx2.1\text{-}Cre}$ mice via intraperitoneal (i.p.) injection every 3 days for 15 days. Like FGF21 treatment, both DIO WT and DIO KLB$^{Nkx2.1\text{-}Cre}$ mice exhibited similar weight reductions in response to PF-05231023 administration (Figures 1E and 1F). Together, these data indicate that FGF21 signaling to the hypothalamus is not necessary for FGF21 to reduce body weight.

To determine if FGF21 signaling to the hypothalamus is sufficient to drive body weight reduction, we generated mice that express KLB only in the hypothalamus by administering Cre recombinase to the hypothalamus of KLB loxTB mice. As described previously,[50] KLB loxTB mice lack endogenous KLB expression due to a loxP-flanked transcription blocker (loxTB). However, in the presence of Cre recombinase, endogenous KLB expression is restored (Figure 1G, KLB loxTB). Weight-matched WT and KLB loxTB mice were transduced with Cre (AAV-CMV-Cre-eGFP) or a control virus (AAV-CMV-eGFP) into the hypothalamus (Figures S1C and S1D) and subsequently administered vehicle or FGF21 via osmotic minipumps for 14 days (Figure 1H). As expected, administration of FGF21 resulted in a significant reduction in body weight of DIO WT mice (Figures 1I and 1J). In contrast, FGF21 treatment in both KLB loxTB mice and KLB loxTB mice with Cre-induced KLB re-expression specifically in the hypothalamus resulted in no detectable weight loss (Figure 1I and 1J). No significant changes in home cage food intake were observed following FGF21 treatment (Figure S1E). These data reveal that FGF21 signaling to the hypothalamus is not sufficient to mediate FGF21's effects on body weight.

Pharmacological FGF21 signaling to the NTS/AP is both required and sufficient for its effect to reduce body weight

KLB-expressing Vglut2$^+$ neurons are also found in the hindbrain, primarily in the NTS and AP, which are well characterized for their roles in energy balance and body weight regulation.[29,32] To

Figure 1. Pharmacological FGF21 signaling to the hypothalamus is not required or sufficient to promote weight loss in DIO mice

(A–D) Diet-induced obese (DIO) WT and KLB$^{Nkx2.1-Cre}$ (KLB$^{fl/fl}$; Nkx2.1-Cre) mice (16–18 weeks old) were administered vehicle or FGF21 (1 mg/kg/day) by osmotic minipump for 14 days (n = 9–13 per group). (A) Plasma FGF21 levels, (B) starting body weights, (C) daily percent change in body weight, and (D) final percent change in body weight.

(E and F) DIO WT and KLB$^{NKX2.1-Cre}$ mice (16–18 weeks old) were administered vehicle or PF-05231023 (i.p. 3 mg/kg) every 3 days for 15 days (n = 8–11 per group). (E) Daily percent change in body weight and (F) final percent change in body weight.

(G–J) DIO WT and KLB loxTB (KLB$^{loxTB/loxTB}$) mice (16–18 weeks old) were injected with AAV-CMV-Cre-EGFP (KLB^{loxTB}; Cre) or AAV-CMV-eGFP (KLB^{loxTB}; GFP) in the hypothalamus and administered vehicle or FGF21 (1 mg/kg/day) by osmotic minipump for 14 days (n = 6–13 per group). (G) Schematic illustration of the viral targeting strategy to restore endogenous KLB expression specifically in the hypothalamus, (H) plasma FGF21 levels, (I) daily percent change in body weight, and (J) final percent change in body weight of mice in (G)–(J).

Values are presented as mean ± SEM. *p < 0.05. Statistical analyses were conducted using Student's t test (B) or two-way ANOVA (C–F, I, and J) with Holms-Sidak's multiple comparison test.

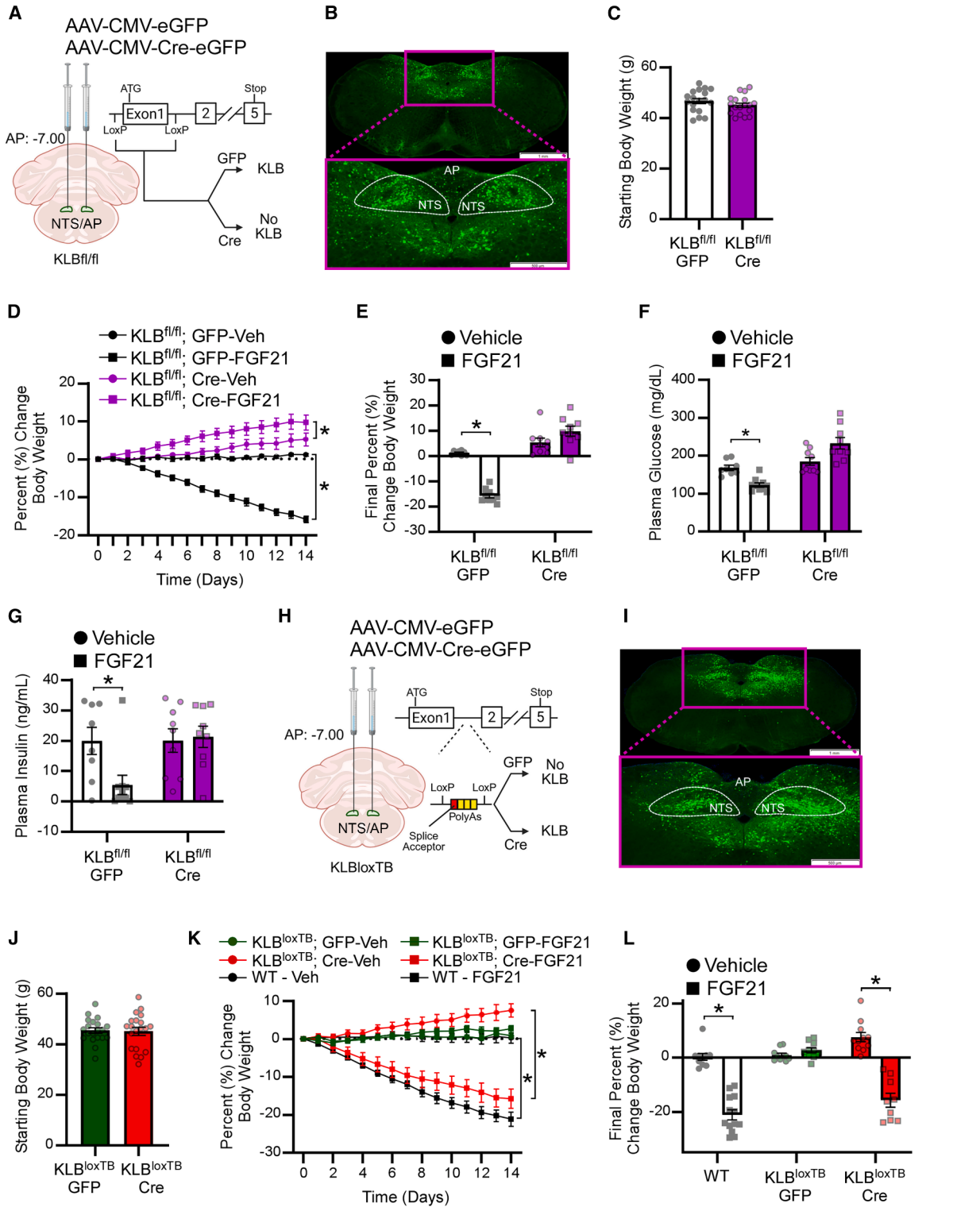

Figure 2. Pharmacological FGF21 signaling to the NTS/AP is both required and sufficient to promote weight loss in DIO mice

(A–G) Diet-induced obese (DIO) KLB$^{fl/fl}$ mice (16–18 weeks old) were injected with AAV-CMV-Cre-EGFP (KLB$^{fl/fl}$; Cre) or AAV-CMV-eGFP (KLB$^{fl/fl}$; GFP) in the nucleus of the solitary tract (NTS) and area postrema (AP) and administered vehicle or FGF21 (1 mg/kg/day) by osmotic minipump for 14 days (n = 8–10 per group). (A) Schematic illustration of the viral targeting strategy to ablate KLB expression specifically in NTS/AP, (B) representative fluorescent image for viral targeting.

(legend continued on next page)

investigate whether FGF21 signaling to the NTS/AP is required for its effect to reduce body weight, we generated mice that lack KLB in the NTS/AP ($KLB^{NTS/AP-KO}$) by administration of AAV-Cre into the NTS/AP (primarily the NTS) of DIO $KLB^{fl/fl}$ mice (Figures 2A and 2B).[18] RNAscope *in situ* hybridization revealed a marked reduction in *Klb* mRNA signal in the NTS of DIO $KLB^{fl/fl}$ mice administered AAV-Cre compared to mice administered AAV-EGFP (Figures S2A and S2B). Weight-matched DIO $KLB^{NTS/AP-KO}$ and DIO control $KLB^{fl/fl}$ littermates were administered FGF21 via osmotic minipumps for 14 days (Figures 2C and S2C). As expected, FGF21 treatment significantly reduced body weight in control $KLB^{fl/fl}$ mice (Figure 2D and 2E). However, ablation of KLB in the NTS/AP completely blocked FGF21-mediated weight loss, suggesting that FGF21 signaling to the NTS/AP is required to reduce body weight (Figure 2D and 2E). There was also a slight increase in food intake in $KLB^{NTS/AP-KO}$ mice following FGF21 administration (Figure S2D), which could be secondary to a slight increase in body weight. Like previous studies,[29] FGF21 treatment induced thermogenic gene expression in the BAT of $KLB^{fl/fl}$ mice, and this induction was prevented by NTS/AP KLB ablation (Figure S2E). Consistent with its effects on body weight, FGF21 administration also significantly reduced plasma glucose and insulin levels in DIO $KLB^{fl/fl}$ but not DIO $KLB^{NTS/AP-KO}$ mice (Figure 2F and 2G).

To explore whether FGF21 signaling to the NTS/AP is sufficient for FGF21-mediated body weight reduction, we administered AAV-GFP or AAV-Cre into the NTS/AP of weight-matched DIO KLB loxTB mice and restored *Klb* mRNA expression in the NTS/AP (Figures 2H–2J, S2F, and S2G). The expression of the physiological levels of KLB in the NTS/AP restored FGF21's ability to reduce body weight, comparable to the weight loss observed in DIO WT mice (Figures 2K and 2L). Consistent with the restoration of body weight responses to FGF21, NTS/AP KLB re-expression also restored FGF21's ability to reduce plasma glucose and insulin levels (Figures S2H and S2I). In addition, restoration of FGF21 signaling to the NTS/AP rescued FGF21's ability to induce BAT thermogenic gene expression (Figure S2J). Finally, the re-expression of KLB restored the ability of FGF21 to reduce hepatic triglyceride levels (Figure S2K). This is consistent with our previous report demonstrating a central mechanism mediating FGF21-induced reductions in hepatic triglycerides.[51] Together, these data indicate that FGF21 signaling in the NTS/AP is sufficient for FGF21-mediated induction of thermogenic gene expression and reduction in body weight.

Pharmacological FGF21 increases firing of NTS Vglut2$^+$ neurons, SNA to BAT, and energy expenditure

Previous work from our lab has demonstrated that FGF21 affects neuronal activity by increasing the activation and excitability of neurons in the VMH, as well as in basolateral amygdala neurons that project to the nucleus accumbens.[31,50] To explore how FGF21 affects neuronal activity in the NTS, we utilized KLB-Cre; Vglut2-IRES-Flp; Ai65-tdTomato triple-knockin mice as previously described.[29] Acute brain slices were prepared, and cell-attached recordings from tdTomato$^+$ cells (KLB^+ $Vglut2^+$) were performed in lean and DIO triple-knockin mice under synaptic blockade (CNQX, AP5, and PTX) (Figure 3A). While consumption of an obesogenic diet reduced baseline firing of KLB^+ $Vglut2^+$ neurons in the NTS, FGF21 application significantly increased the firing frequency of these neurons in both lean and DIO triple-knockin mice (Figures 3B and 3C). Thus, consistent with FGF21's effects on KLB^+ neurons in the VMH, FGF21 also activates the KLB^+ $Vglut2^+$ neurons in the NTS under both lean and DIO conditions.

As previously reported, FGF21's effects on body weight are primarily due to an increase in energy expenditure in rodents.[29,52] To explore whether FGF21 signaling to the NTS/AP is required for its effect on energy expenditure, DIO $KLB^{fl/fl}$ and DIO $KLB^{NTS/AP-KO}$ mice were first housed in metabolic cages (Promethion) for 5 days for baseline measurements of energy expenditure (Figures 3D and S3A). Next, mice were administered FGF21 via osmotic minipump for 14 days and were housed in metabolic cages for the last 5 days of FGF21 administration (Figure 3D). As expected, no difference in baseline energy expenditure was observed between DIO $KLB^{fl/fl}$ and DIO $KLB^{NTS/AP-KO}$ mice (Figure 3E and 3F). However, while FGF21 administration significantly elevated energy expenditure in the DIO $KLB^{fl/fl}$ mice, FGF21 failed to elevate energy expenditure in DIO $KLB^{NTS/AP-KO}$ mice (Figures 3E and 3F). Consistent with the metabolic cage data, $KLB^{NTS/AP-KO}$ abolished FGF21-mediated induction of thermogenic gene expression (Figure 3G). Together, these data indicate that FGF21 signaling to the NTS/AP is required for FGF21 to induce energy expenditure.

FGF21 can act on the CNS to stimulate sympathetic nerve activity (SNA) in BAT.[30] To explore if NTS/AP FGF21 signaling is required for this sympathoexcitation effect, we recorded SNA to BAT in anesthetized DIO $KLB^{fl/fl}$ and DIO $KLB^{NTS/AP-KO}$ mice following vehicle or FGF21 treatment (Figures 3H, 3I, and S3B). As expected, FGF21 administration resulted in significantly elevated BAT SNA in DIO $KLB^{fl/fl}$ but not DIO $KLB^{NTS/AP-KO}$ mice (Figures 3H, 3I, and S3C), suggesting that FGF21 signaling to the NTS/AP is required for its effect to increase BAT SNA.

To investigate whether the activation of NTS/AP KLB^+ neurons is sufficient to increase energy expenditure, we expressed a human M3 muscarinic designer receptor exclusively activated by designer drugs (DREADD; hM3Dq) in the hindbrain KLB^+ neurons by administering an AAV-hSyn-DIO-hM3Dq-mCherry into the hindbrain of DIO KLB-Cre mice (Figure S3D). Control DIO

Scale bars, 1 mm for overview (top) and 500 μm for zoom in (bottom). (C) Starting body weight, (D) daily percent change in body weight, (E) final percent change in body weight, (F) plasma glucose level, and (G) plasma insulin level.

(H–L) DIO WT or KLB loxTB ($KLB^{loxTB/loxTB}$) mice (16–18 weeks old) were injected with AAV-CMV-Cre-EGFP (KLB^{loxTB}; Cre) or AAV-CMV-eGFP (KLB^{loxTB}; GFP) in NTS/AP and administered vehicle or FGF21 (1 mg/kg/day) by osmotic minipump for 14 days (n = 9–13 per group). (H) Schematic illustration of the viral targeting strategy to restore endogenous KLB expression specifically in NTS/AP. (I) Representative fluorescent image for viral targeting. Scale bars, 1 mm for overview (top) and 500 μm for zoom in (bottom). (J) Starting body weight, (K) daily percent change in body weight, and (L) final percent change in body weight.

Values are presented as mean ± SEM. *$p < 0.05$. Statistical analyses were conducted using Student's t test (C and J) and two-way ANOVA (D–G, K, and L) with Holms-Sidak's multiple comparison test.

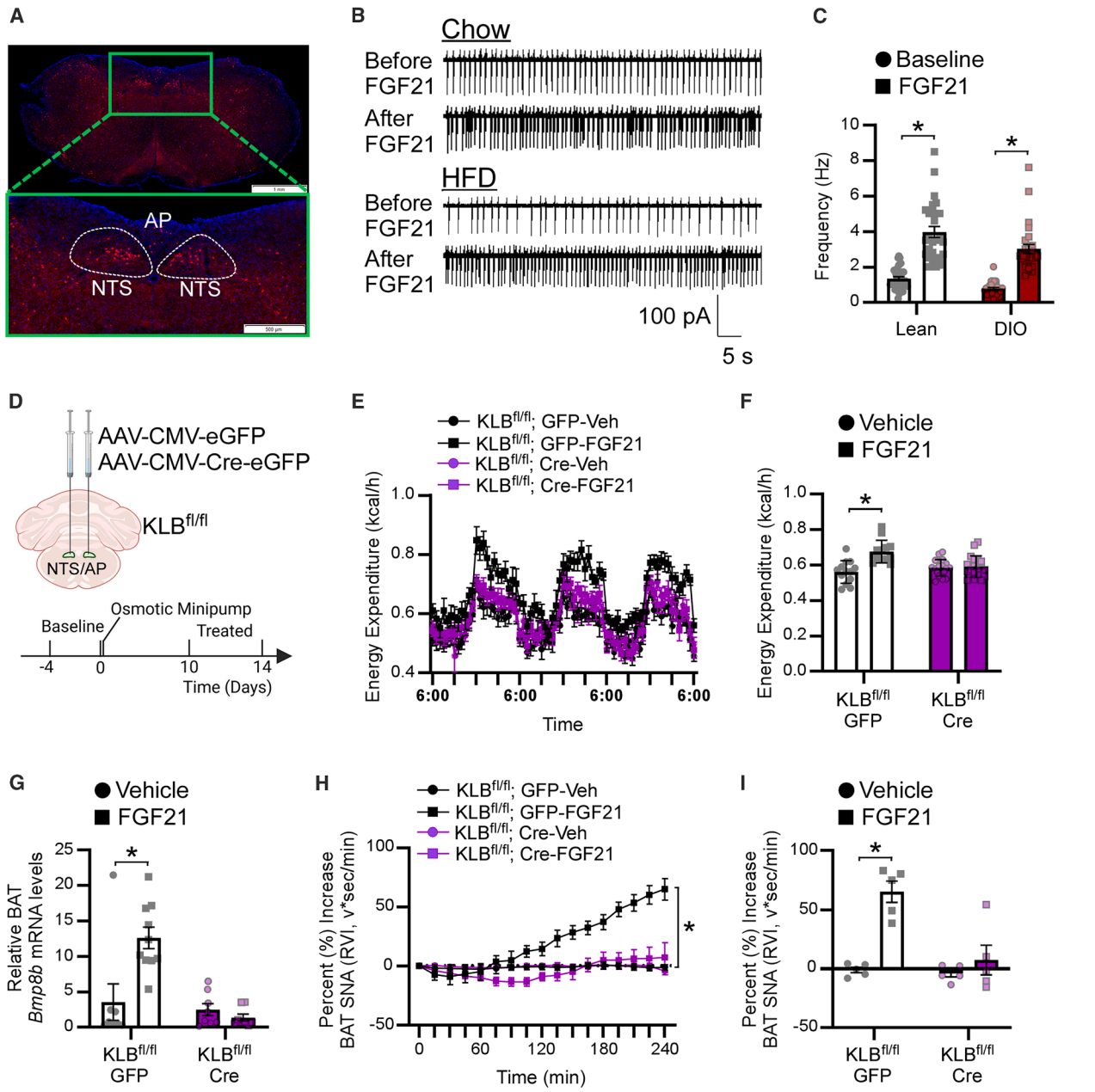

Figure 3. FGF21 signaling in the NTS/AP activates KLB^{+}Vglut2^{+} neurons and is required for pharmacological FGF21-mediated potentiation of brown fat SNA and energy expenditure

(A–C) Patch clamp recording of tdTomato^{+} nucleus of the solitary tract (NTS) neurons for 16–18-week-old diet-induced obese (DIO) or lean KLB-Cre; Vglut2-FLP; Ai65-tdTomato triple-knockin mice, before or after bath application of FGF21 (50 ng/mL) (25–32 cells per group). (A) Fluorescent image of NTS/AP KLB^{+}/Vglut2^{+}/tdTomato+ neurons. Scale bars, 1 mm for overview (top) and 500 μm for zoom-in (bottom). (B) Representative traces of neural firing and (C) firing frequencies. (D–F) Energy expenditure of 16–18-week-old DIO KLB$^{fl/fl}$ mice injected with AAV-CMV-Cre-EGFP (KLB$^{fl/fl}$; Cre) or AAV-CMV-eGFP (KLB$^{fl/fl}$; GFP) in the NTS and area postrema (AP), presented as baseline (day −2 to 0) and during FGF21 (1 mg/kg/day) administration by osmotic minipump (days 12–14) (n = 13–19 per group). (D) Schematic illustration of viral targeting strategy to ablate KLB expression in NTS/AP and the experimental timeline, (E) hourly energy expenditure, and (F) average energy expenditure.

(G) Relative BAT *Bmp8b* mRNA level in 16–18-week-old DIO KLB$^{fl/fl}$; Cre or KLB$^{fl/fl}$; GFP mice treated with vehicle or FGF21 (1 mg/kg/day) by osmotic minipump for 14 days (n = 8–10 per group).

(H and I) Sympathetic nerve activity (SNA) to brown adipose tissue (BAT) in 16–18-week-old DIO KLB$^{fl/fl}$; Cre or KLB$^{fl/fl}$; GFP mice treated with vehicle or FGF21 (i.v. 1 mg/kg; n = 5 per group). (H) Percent change in BAT SNA and (I) final change in BAT SNA.

Values are presented as mean ± SEM. *$p < 0.05$. Statistical analyses were conducted using two-way ANOVA with Holms-Sidak's multiple comparison test.

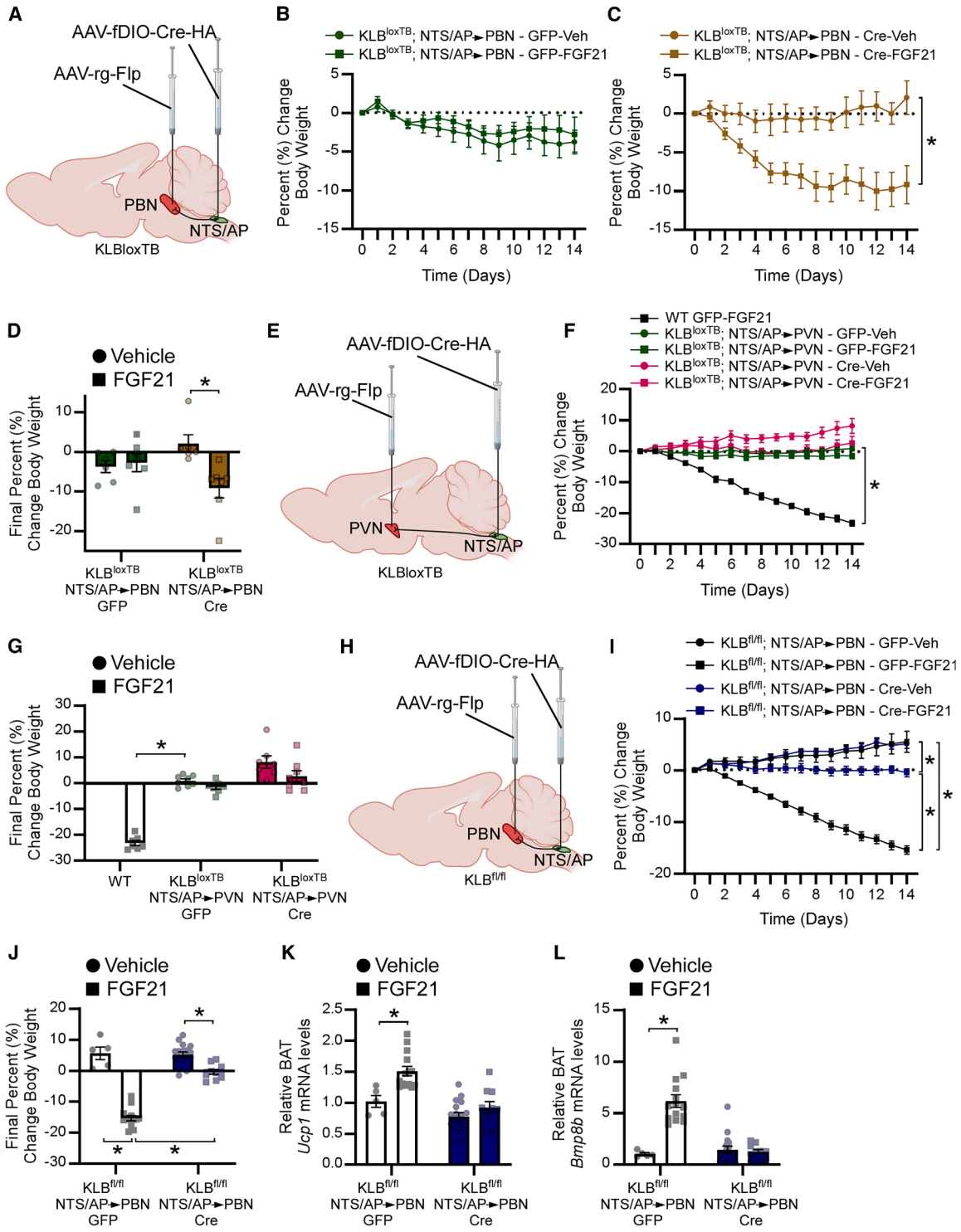

Figure 4. FGF21 action in NTS/AP neurons that project to the PBN, but not to the PVN, is both necessary and sufficient to promote weight loss in DIO mice

(A–D) Diet-induced obese (DIO) KLB loxTB ($KLB^{loxTB/loxTB}$) mice (16–18 weeks old) were injected with rgAAV-EF1a-Flpo (KLB^{loxTB}; NTS/AP→PBN-Cre) or rgAAV-hSyn-DIO-EGFP (KLB^{loxTB}; NTS/AP→PBN-GFP) into the parabrachial nucleus (PBN) and AAV-EF1a-fDIO-Cre into the nucleus of the solitary tract (NTS) and area postrema (AP), and then administered vehicle or FGF21 (1 mg/kg/day) by osmotic minipump for 14 days (n = 6–7 per group). (A) Schematic illustration of viral targeting strategy to restore endogenous KLB expression specifically in PBN-projecting NTS/AP neurons. (B and C) Daily percent change in body weight in KLB^{loxTB}; NTS/AP→PBN-GFP (B) and KLB^{loxTB}; NTS/AP→PBN-Cre (C), and (D) final percent change in body weight.

(legend continued on next page)

KLB-Cre mice received an AAV-hSyn-DIO-mCherry. Baseline energy expenditure was measured in metabolic cages, followed by chemogenetic activation of hindbrain KLB$^+$ neurons with deschloroclozapine dihydrochloride (DCZ) administered in drinking water. Surprisingly, chemogenetic activation of the hindbrain KLB$^+$ neurons did not result in visible changes in energy expenditure (Figure S3E). To exclude insufficient receptor engagement as a confounding factor, DCZ was subsequently delivered i.p. at a dose that robustly activates the hM3Dq-expressing neurons.[53] Despite the increased dose of DCZ administration, no difference was observed between chemogenetic activation and controls (Figure S3F). Importantly, intraperitoneal administration of DCZ resulted in robust cFos induction, supporting effective chemogenetic activation (Figures S3G and S3H). Together, these findings indicate that the activation of hindbrain KLB$^+$ neurons is not sufficient to drive energy expenditure induced by FGF21.

To explore whether activation of KLB$^+$ neurons in the hindbrain is sufficient to increase BAT sympathetic input, we independently recorded SNA to BAT in anesthetized DIO KLB-Cre mice expressing hM3Dq or mCherry in hindbrain KLB$^+$ neurons. After achieving a stable baseline, mice were given clozapine-N-oxide (CNO) or saline as previously described[54] to activate the hindbrain KLB$^+$ neurons. Consistent with the energy expenditure data (Figures S3D–S3H), chemogenetic activation of hindbrain KLB$^+$ neurons did not increase BAT SNA (Figure S3I). Therefore, although FGF21 signaling increases the activation of glutamatergic KLB+ NTS/AP neurons, the chemogenetic activation of all KLB+ NTS/AP neurons is not sufficient to drive BAT SNA.

PBN-projecting neurons in the NTS/AP are responsible for pharmacological FGF21-mediated body weight reduction

The NTS/AP projects to multiple brain regions implicated in the regulation of energy balance.[33] For further insight on how FGF21 signaling in the NTS/AP influences energy expenditure and weight loss, we mapped NTS/AP KLB$^+$ neuron projections by injecting an AAV-FLEX-tdTomato-expressing virus into the NTS/AP of KLB-Cre mice (Figures S4A and S2B). We found that KLB$^+$ NTS/AP neurons innervate the brain areas that are linked to energy homeostasis, including the PBN, PVN, the bed nucleus of stria terminalis (BNST), and LH (Figure S4C). Interestingly, the PBN was most robustly innervated by NTS/AP^{KLB} neurons. To determine if these PBN-projecting neurons are sufficient for FGF21 to reduce body weight, we injected a retrograde AAV-FLP virus into the PBN and a Flp-dependent Cre virus into the NTS/AP of KLB loxTB mice, enabling Cre expression, and therefore KLB re-expression specifically in PBN-projecting NTS/AP neurons (NTS/AP→PBN) (Figures 4A and S4D). FGF21 treatment via osmotic minipump significantly reduced body weight in KLB$^{NTS/AP→PBN}$ re-expression mice but not in littermates receiving a control retrograde AAV-GFP-expressing virus into the PBN (Figures 4B–4D). The degree of weight loss is comparable to other experiments in this paper (e.g., Figures 1C and 1I) and other papers.[55] In addition, and importantly, the degree of weight loss is comparable to that of mice in which KLB expression is restored to the NTS/AP of KLB loxTB mice (Figures 2K and 2L), which are on a mixed genetic background. No change in food intake was observed following FGF21 administration (Figure S4E). These data suggest that PBN-projecting NTS/AP KLB$^+$ neurons are sufficient for the body weight-reducing effects of NTS/AP FGF21 signaling. To evaluate the role of other NTS/AP KLB$^+$ neural projections in mediating the weight loss effects of FGF21, we next targeted PVN-projecting NTS/AP neurons in DIO KLB loxTB mice using a similar approach (Figures 4E and S4F). Unlike PBN-projecting neurons, restoration of KLB expression in PVN-projecting NTS/AP neurons did not rescue the weight loss associated with FGF21 administration (Figure 4F and 4G), indicating that PVN-projecting NTS/AP neurons are not sufficient to drive the effect of FGF21 to reduce body weight. No significant differences in food intake were observed (Figure S4G).

To investigate whether FGF21 signaling to NTS/AP PBN-projecting neurons is required for its effect on body weight, we performed the same intersectional approach in KLB$^{fl/fl}$ mice, resulting in KLB deletion specifically from NTS/AP neurons that project to the PBN (Figures 4H and S4H). Consistent with KLB$^{NTS/AP-KO}$ mice, FGF21-mediated weight loss was significantly attenuated in mice with KLB deletion from NTS/AP→PBN neurons (KLB$^{fl/fl}$; NTS/AP→PBN-Cre), as compared with control-injected mice (KLB$^{fl/fl}$; NTS/AP→PBN-GFP). This indicates that PBN-projecting NTS/AP neurons are required for most of the FGF21-induced weight loss (Figures 4I and 4J). In addition to preventing body weight loss, KLB$^{NTS/AP→PBN}$ knockout also abolished FGF21-mediated activation of BAT thermogenic gene expression (Figures 4K and 4L). No significant change in food intake was observed following FGF21 treatment (Figure S4I). Together, these data demonstrate that PBN-projecting NTS/AP KLB$^+$ neurons are required for pharmacologically administered FGF21 to exert most of its effect to induce energy expenditure and promote weight loss.

DISCUSSION

In this study, we reveal the central target of pharmacological FGF21 to reduce body weight. We demonstrate that the NTS/AP, and not the hypothalamus, is both required and sufficient

(E–G) DIO WT and KLB loxTB (KLB$^{loxTB/loxTB}$) mice (16–18 weeks old) were injected with rgAAV-EF1a-Flpo (KLB^{loxTB}; NTS/AP→PVN-Cre) or rgAAV-hSyn-DIO-EGFP (KLB^{loxTB}; NTS/AP→PVN-GFP) into the paraventricular nucleus of the hypothalamus (PVN) and AAV-EF1a-fDIO-Cre into NTS/AP and administered vehicle or FGF21 (1 mg/kg/day) by osmotic minipump for 14 days (n = 7–8 per group). (E) Schematic illustration of viral targeting strategy to restore endogenous KLB expression specifically in NTS/AP PVN-projecting neurons, (F) daily percent change in body, and (G) final percent change in body weight.
(H–L) DIO KLB$^{fl/fl}$ mice were injected with rgAAV-EF1a-Flpo (KLB$^{fl/fl}$; NTS/AP→PBN-Cre) or rgAAV-hSyn-DIO-EGFP (KLB$^{fl/fl}$; NTS/AP→PBN-GFP) (16–18 weeks old) into the PBN and AAV-EF1a-fDIO-Cre into NTS/AP and administered vehicle or FGF21 (1 mg/kg/day) by osmotic minipump for 14 days (n = 5–17 per group). (H) Schematic illustration of viral targeting strategy to ablate KLB expression specifically in NTS/AP PBN-projecting neurons, (I) daily percent change in body weight, (J) final percent change in body weight, (K) relative *Ucp1* mRNA level in the brown adipose tissue (BAT), and (L) relative *Bmp8b* mRNA level in BAT. Values are presented as mean ± SEM. *$p < 0.05$. Statistical analyses were conducted using two-way ANOVA with Holms-Sidak's multiple comparison test.

for FGF21-mediated weight loss. Specifically, pharmacologically administered FGF21 activates the NTS/AP KLB$^+$ neurons and induces BAT SNA and energy expenditure to reduce body weight. Furthermore, the observed changes in energy expenditure and body weight are largely attributable to NTS/AP neurons that project to the PBN, but not PVN.

The hindbrain, specifically the NTS and AP, has received considerable attention as regulators of energy homeostasis.[56] Despite most studies focusing on their role in satiety, previous data have alluded to a role for these hindbrain regions in the regulation of energy expenditure.[41,42,57,58] However, direct evidence for NTS and AP neurons to promote energy expenditure is still lacking. Here, we identified a neural population in NTS/AP that is activated by the pharmacological FGF21 treatment, promotes energy expenditure, and reduces body weight without lowering food intake. Notably, we unexpectedly discovered that pharmacological FGF21 administration does not regulate body weight by acting directly in the hypothalamus, a region that has long been considered the target for FGF21 action to regulate energy homeostasis. Although KLB$^+$ glutamatergic neurons are found in several hypothalamic regions known for controlling energy expenditure, including the PVN, VMH, DMH, and LH,[29] these hypothalamic regions are not necessary or sufficient for FGF21-mediated weight loss. This is consistent with our previous finding that VMH KLB$^+$ neurons are not responsible for FGF21-induced weight loss, despite their prominent role in FGF21-mediated suppression of sucrose intake.[31] Furthermore, re-expression of KLB in NTS/AP neurons also restored FGF21-mediated reduction in hepatic triglycerides. This is consistent with an earlier report demonstrating a central mechanism of FGF21-mediated reductions in hepatic triglycerides,[51] and highlighting the NTS/AP as the brain region mediating such effects. However, as these studies did not include diets that promote metabolic-associated steatohepatitis (MASH) (i.e., GAN or FPC diet),[51] additional research is needed to determine the involvement of this circuit in mediating FGF21's effects to reverse hepatic fibrosis. In addition, whether NTS/AP KLB-expressing neurons are also responsible for the physiological functions of FGF21 on energy balance, or other metabolic functions of FGF21, requires further investigation.

Following KLB ablation in the NTS/AP, we noted an unexpected increase in food intake and body weight following FGF21 administration. This slight yet significant increase in body weight and food intake might be attributable to the action of FGF21 in the brain areas other than the hindbrain. When a WT animal receives FGF21, FGF21 signaling in the hindbrain stimulates robust body weight reductions, and any potential effect of FGF21 on other brain regions could be masked. Importantly, no increase in body weight and food intake was observed in KLB loxTB animals expressing EGFP in the NTS/AP. Consistent with our data, another study observed increased body weight, body fat content, and a trend toward increased food intake in FGF21-transgenic mice that lack KLB expression in Camk2a$^+$ neurons, indicating that FGF21 could have effects on other types of neurons.[30]

Our finding that FGF21 signaling to the hindbrain and not the hypothalamus is required for its effects to lower body weight is unexpected based on a previous study that crossed KLB$^{fl/fl}$ mice to Phox2b-Cre mice,[59] which is supposed to delete KLB from the NTS. That study reported that deletion of KLB from Phox2b-Cre cells (KLB$^{fl/fl}$; Phox2b-Cre) did not block the reduced body weight of FGF21 transgenic mice.[60] However, those studies did not report KLB deletion from the hindbrain.[60] Notably, using deposited NTS datasets,[37,61] we find that there are KLB neurons in the NTS which do not express Phox2b and therefore would not eliminate FGF21 signaling in this region.

Previously, we demonstrated that FGF21-mediated weight loss was attenuated when KLB was deleted from LepR-expressing neurons. LepR neurons are well documented within discrete hindbrain nuclei, including the NTS/AP, and the spatial distribution of LepR neurons partially overlaps with KLB$^+$ Vglut2$^+$ neurons.[62] Our findings are therefore most consistent with the interpretation that at least a subset of LepR-expressing neurons within the hindbrain contributes to the KLB-dependent effects of FGF21 on body weight and energy expenditure. Future studies are needed to resolve LepR and KLB co-expression at single-cell resolution and the potential involvement of hindbrain LepR$^+$/KLB$^+$ neurons in FGF21-mediated weight loss and thermogenesis.

In this paper, we demonstrate that FGF21-induced increases in SNA to BAT and BAT thermogenesis depend on KLB signaling in the hindbrain. However, previous studies have also shown that FGF21 can reduce body weight and improve glucose homeostasis independent of UCP1.[52,63–66] However, it is important to note that BAT can regulate energy expenditure independent of UCP1, and loss of UCP1 does not abolish BAT thermogenesis.[67,68] Nevertheless, as we noted previously,[14] while FGF21's primary mode of action is to increase energy expenditure through adipose thermogenesis, if this pathway is disrupted, then alternative mechanisms can be employed to promote weight loss. Critically, the hindbrain KLB-dependent circuit we have identified in this study is required for any effect of FGF21 on body weight reduction, and may represent an upstream regulatory node to regulate whole-body energy balance. Further research is needed to fully delineate the complex effects of FGF21 action on body weight and energy homeostasis.

A surprising result from these studies is that while FGF21 administration activates glutamatergic KLB$^+$ neurons in the NTS/AP, chemogenetic activation of all NTS/AP KLB$^+$ neurons is not sufficient to trigger the elevations in energy expenditure and BAT SNA observed with FGF21 administration. The effect of FGF21 signaling in hindbrain neurons to regulate energy expenditure and SNA may involve other known cellular functions of FGF21, such as changes in gene expression or activation of unique phosphorylation cascades. Alternatively, the effect of FGF21 on neuronal firing (i.e., firing rate, neurotransmitter release, synaptic plasticity, etc.) may not fully be recapitulated by an activating DREADD.

Neurons in the NTS/AP project to a number of brain regions regulating energy homeostasis.[69] However, most of this research has focused on NTS/AP projections that regulate food consumption.[33,70] Our tracing experiments revealed that NTS/AP KLB$^+$ neurons project to multiple brain areas implicated in the regulation of BAT thermogenesis, with the most prominent axonal projections in the PBN. While excitatory NTS/AP projections to the PBN have been established to regulate feeding

behavior,[33] less is known about NTS/AP → PBN circuits regulating energy expenditure. Previous work suggests that projections from the NTS to the PBN can regulate thermogenesis in response to environmental temperature.[71,72] However, we demonstrate for the first time that the recruitment of PBN-projecting NTS/AP neurons by FGF21 can induce BAT thermogenic gene expression and promote weight loss. Future studies are required to fully characterize the role of this NTS/AP→PBN projection in the regulation of energy expenditure with indirect calorimetry. NTS/AP KLB^{+} neurons also project to other brain regions that regulate energy expenditure, including the PVN. Although a majority of PVN neurons project to the BAT,[73,74] activation or disinhibition of PVN neurons reverses BAT SNA increases evoked by cooling, likely by activating GABAergic neurons in the raphe pallidus (RPa).[75] Given the glutamatergic nature of KLB^{+} neurons that regulate energy expenditure and body weight,[29] it seems unlikely that NTS/AP KLB^{+} neurons would act on the PVN to promote energy expenditure and weight loss. Indeed, re-expression of KLB specifically in PVN-projecting NTS/AP neurons did not restore weight loss associated with FGF21 treatment.

While the hypothalamus is not a direct target of KLB$^{NTS/AP}$ neurons in FGF21-mediated weight loss, multiple hypothalamic pathways could be recruited by the NTS/AP→PBN circuit following pharmacological FGF21 treatment. Indeed, PBN neurons project to the median preoptic nucleus (MnPO)[76] and likely disinhibit BAT thermogenesis by suppressing GABAergic medial preoptic area neurons.[77] Recently, a PBN→DMH circuit has been identified that functions parallel to the PBN→POA pathway to promote the thermogenic response to cold.[78] Whether one or multiple of these pathways, or an yet unknown pathway, are recruited by FGF21-mediated activation of the KLB$^{NTS/AP→PBN}$ pathway to reduce body weight requires further investigation.

Finally, our data on the ability of KLB$^{NTS/AP→PBN}$ neurons to drive BAT thermogenic gene expression and weight loss following FGF21 treatment provide valuable insights into the therapeutic applications of FGF21. The NTS and AP are targeted by multiple pharmacological agents for obesity treatment, including GLP-1 analogs.[39] However, most of these agents signal to neurons in the NTS and AP that suppress food intake.[6,11,79] Attempts for weight loss by reducing food intake are often associated with a chronic reduction in energy expenditure,[11,13] which limits the efficacy of treatment and leads to weight regain following drug discontinuation.[6,8,12] The mechanisms for this reduction in energy expenditure are unclear, but it is likely a compensatory response to maintain body weight. FGF21 has been shown to enhance the effects of leptin and GLP-1 analogs on weight loss[80,81]; thus, co-administration of FGF21 with therapeutics that minimize food consumption may be promising for more potent weight loss, as well as longer-lasting effects to maintain weight loss. While efforts have been made to develop therapeutics that boost energy expenditure, off-target signaling limits their use.[82] Here, we detail a highly specific neural pathway that could induce energy expenditure, improve glucose homeostasis and insulin sensitivity, and lower body weight independent of food intake. Future research is warranted to explore the therapeutic value of targeting the KLB$^{NTS/AP→PBN}$ pathway for weight loss therapeutics. Furthermore, although we illustrated mechanistically that FGF21 signaling to the hindbrain mediates its effect in promoting energy expenditure, whether there is a long-lasting benefit in energy expenditure following FGF21 treatment remains unclear and requires further investigations.

Limitations of the study

The experiments in this study were performed in mice, and the quantitative contribution of energy expenditure to body weight regulation may differ between rodents and humans. As such, future studies will be needed to explore the effects of FGF21 action under thermoneutral conditions. In addition, these studies used only male mice, as female mice do not gain as much weight on a high-fat diet, which precludes sex-stratified analyses. Additionally, while our findings demonstrate that NTS/AP KLB signaling is required for FGF21-mediated decreases in body weight, the precise downstream effector tissues and molecular mechanisms contributing to this response were not fully delineated. Finally, although we establish that FGF21-mediated energy expenditure requires hindbrain signaling, additional studies are necessary to confirm that projections from NTS/AP to PBN functionally alter energy expenditure beyond changes in thermogenic gene expression. Some figures included illustrations made using BioRender.com.

RESOURCE AVAILABILITY

Lead contact

Further information and requests for resources and reagents should be directed to and will be fulfilled by the lead contact, Matthew J. Potthoff (matthew-potthoff@ou.edu).

Materials availability

This study did not generate new, unique reagents.

Data and code availability

- Data reported in this paper will be shared by the lead contact upon request.
- This paper does not report original code.
- Any additional information required to reanalyze the data reported in this paper is available from the lead contact upon request.

ACKNOWLEDGMENTS

We thank Dr. Birgitte Andersen (Novo Nordisk) for providing FGF21 protein. We thank Pfizer for providing PF-05231023. We thank Dr. Jon Resch (University of Iowa) for experimental input and expertise. This work is funded by the National Institutes of Health (NIH) R01DK106104 (M.J.P.), Veterans Affairs Merit Review program I01BX004634 (M.J.P.), and K01DK133667 (K.E.C.). K.R. is supported by the National Institutes of Health (R01 HL162773 and R01 HL172944) and the US Department of Veterans Affairs (I01 BX004249 and IK6 BX006040). The authors would like to acknowledge the use of the University of Iowa Central Microscopy Research Facility, the University of Iowa Metabolic Phenotyping Core, and the Genomics Division of the Iowa Institute of Human Genetics.

AUTHOR CONTRIBUTIONS

Y.L. and K.E.C. designed and performed the experiments, interpreted data, and wrote the paper. I.A., A.I.S., M.C.R., D.A.M., and K.R. performed the experiments and interpreted the data. M.J.P. conceived the project, designed the experiments, interpreted the data, wrote the paper, and is responsible for the integrity of its content.

DECLARATION OF INTERESTS

The authors declare no competing interests.

STAR★METHODS

Detailed methods are provided in the online version of this paper and include the following:

- KEY RESOURCES TABLE
- EXPERIMENTAL MODEL AND STUDY PARTICIPANT DETAILS
  - Animals
- METHOD DETAILS
  - Administration of recombinant FGF21
  - Administration of PF-05231023
  - Surgery
  - Whole organ clearing
  - AAV viral constructs
  - Gene expression
  - Electrophysiology
  - RNAscope *in situ* hybridization
  - Immunohistochemistry
  - Indirect calorimetry
  - Home cage food intake
  - Sympathetic nerve recordings
  - Plasma analyses
  - Hepatic lipid measurement
- QUANTIFICATION AND STATISTICAL ANALYSIS
  - Statistical analysis

SUPPLEMENTAL INFORMATION

Supplemental information can be found online at https://doi.org/10.1016/j.celrep.2026.117093.

Received: August 4, 2025
Revised: January 21, 2026
Accepted: February 16, 2026
Published: March 31, 2026

REFERENCES

1. Bluher, M. (2019). Obesity: global epidemiology and pathogenesis. Nat. Rev. Endocrinol. *15*, 288–298. https://doi.org/10.1038/s41574-019-0176-8.
2. Piche, M.E., Tchernof, A., and Despres, J.P. (2020). Obesity Phenotypes, Diabetes, and Cardiovascular Diseases. Circ. Res. *126*, 1477–1500. https://doi.org/10.1161/CIRCRESAHA.120.316101.
3. Avgerinos, K.I., Spyrou, N., Mantzoros, C.S., and Dalamaga, M. (2019). Obesity and cancer risk: Emerging biological mechanisms and perspectives. Metabolism *92*, 121–135. https://doi.org/10.1016/j.metabol.2018.11.001.
4. Li, Y., Pan, A., Wang, D.D., Liu, X., Dhana, K., Franco, O.H., Kaptoge, S., Di Angelantonio, E., Stampfer, M., Willett, W.C., et al. (2018). Impact of Healthy Lifestyle Factors on Life Expectancies in the US Population. Circulation *138*, 345–355. https://doi.org/10.1161/CIRCULATIONAHA.117.032047.
5. Nagi, M.A., Ahmed, H., Rezq, M.A.A., Sangroongruangsri, S., Chaikledkaew, U., Almalki, Z., and Thavorncharoensap, M. (2024). Economic costs of obesity: a systematic review. Int. J. Obes. *48*, 33–43. https://doi.org/10.1038/s41366-023-01398-y.
6. Drucker, D.J. (2025). GLP-1-based therapies for diabetes, obesity and beyond. Nat. Rev. Drug Discov. *24*, 631–650. https://doi.org/10.1038/s41573-025-01183-8.
7. Drucker, D.J. (2025). Discovery of GLP-1-Based Drugs for the Treatment of Obesity. N. Engl. J. Med. *392*, 612–615. https://doi.org/10.1056/NEJMcibr2409089.
8. Drucker, D.J. (2024). Efficacy and Safety of GLP-1 Medicines for Type 2 Diabetes and Obesity. Diabetes Care *47*, 1873–1888. https://doi.org/10.2337/dci24-0003.
9. Alabduljabbar, K., Alsaqaaby, M., Neff, K.J., Crotty, M., and le Roux, C.W. (2024). Weight loss response in patients with obesity treated with injectable semaglutide in a real-world setting. Endocrine *83*, 392–398. https://doi.org/10.1007/s12020-023-03534-0.
10. Webster, C.M., Mittal, N., Dhurandhar, E.J., and Dhurandhar, N.V. (2023). Potential contributors to variation in weight-loss response to liraglutide. Obes. Rev. *24*, e13568. https://doi.org/10.1111/obr.13568.
11. Blundell, J., Finlayson, G., Axelsen, M., Flint, A., Gibbons, C., Kvist, T., and Hjerpsted, J.B. (2017). Effects of once-weekly semaglutide on appetite, energy intake, control of eating, food preference and body weight in subjects with obesity. Diabetes Obes. Metab. *19*, 1242–1251. https://doi.org/10.1111/dom.12932.
12. Grannell, A., Al-Najim, W., and le Roux, C. (2024). Long-term weight outcomes in patients treated with liraglutide 3.0 mg in real-world clinical practice. Clin. Obes. *14*, e12622. https://doi.org/10.1111/cob.12622.
13. van Eyk, H.J., Paiman, E.H.M., Bizino, M.B., IJzermans, S.L., Kleiburg, F., Boers, T.G.W., Rappel, E.J., Burakiewicz, J., Kan, H.E., Smit, J.W.A., et al. (2020). Liraglutide decreases energy expenditure and does not affect the fat fraction of supraclavicular brown adipose tissue in patients with type 2 diabetes. Nutr. Metab. Cardiovasc. Dis. *30*, 616–624. https://doi.org/10.1016/j.numecd.2019.12.005.
14. Flippo, K.H., and Potthoff, M.J. (2021). Metabolic Messengers: FGF21. Nat. Metab. *3*, 309–317. https://doi.org/10.1038/s42255-021-00354-2.
15. Suzuki, M., Uehara, Y., Motomura-Matsuzaka, K., Oki, J., Koyama, Y., Kimura, M., Asada, M., Komi-Kuramochi, A., Oka, S., and Imamura, T. (2008). betaKlotho is required for fibroblast growth factor (FGF) 21 signaling through FGF receptor (FGFR) 1c and FGFR3c. Mol. Endocrinol. *22*, 1006–1014. https://doi.org/10.1210/me.2007-0313.
16. Ogawa, Y., Kurosu, H., Yamamoto, M., Nandi, A., Rosenblatt, K.P., Goetz, R., Eliseenkova, A.V., Mohammadi, M., and Kuro-o, M. (2007). BetaKlotho is required for metabolic activity of fibroblast growth factor 21. Proc. Natl. Acad. Sci. USA *104*, 7432–7437. https://doi.org/10.1073/pnas.0701600104.
17. Kurosu, H., Choi, M., Ogawa, Y., Dickson, A.S., Goetz, R., Eliseenkova, A.V., Mohammadi, M., Rosenblatt, K.P., Kliewer, S.A., and Kuro-O, M. (2007). Tissue-specific expression of betaKlotho and fibroblast growth factor (FGF) receptor isoforms determines metabolic activity of FGF19 and FGF21. J. Biol. Chem. *282*, 26687–26695. https://doi.org/10.1074/jbc.M704165200.
18. Ding, X., Boney-Montoya, J., Owen, B.M., Bookout, A.L., Coate, K.C., Mangelsdorf, D.J., and Kliewer, S.A. (2012). betaKlotho is required for fibroblast growth factor 21 effects on growth and metabolism. Cell Metab. *16*, 387–393. https://doi.org/10.1016/j.cmet.2012.08.002.
19. Coskun, T., Bina, H.A., Schneider, M.A., Dunbar, J.D., Hu, C.C., Chen, Y., Moller, D.E., and Kharitonenkov, A. (2008). Fibroblast growth factor 21 corrects obesity in mice. Endocrinology *149*, 6018–6027. https://doi.org/10.1210/en.2008-0816.
20. Kharitonenkov, A., Shiyanova, T.L., Koester, A., Ford, A.M., Micanovic, R., Galbreath, E.J., Sandusky, G.E., Hammond, L.J., Moyers, J.S., Owens, R.A., et al. (2005). FGF-21 as a novel metabolic regulator. J. Clin. Investig. *115*, 1627–1635. https://doi.org/10.1172/jci23606.
21. Xu, J., Lloyd, D.J., Hale, C., Stanislaus, S., Chen, M., Sivits, G., Vonderfecht, S., Hecht, R., Li, Y.S., Lindberg, R.A., et al. (2009). Fibroblast growth factor 21 reverses hepatic steatosis, increases energy expenditure, and improves insulin sensitivity in diet-induced obese mice. Diabetes *58*, 250–259. https://doi.org/10.2337/db08-0392.
22. BonDurant, L.D., Ameka, M., Naber, M.C., Markan, K.R., Idiga, S.O., Acevedo, M.R., Walsh, S.A., Ornitz, D.M., and Potthoff, M.J. (2017). FGF21 Regulates Metabolism Through Adipose-Dependent and -Independent Mechanisms. Cell Metab. *25*, 935–944.e4. https://doi.org/10.1016/j.cmet.2017.03.005.

23. Andersen, B., Straarup, E.M., Heppner, K.M., Takahashi, D.L., Raffaele, V., Dissen, G.A., Lewandowski, K., Bödvarsdottir, T.B., Raun, K., Grove, K.L., et al. (2018). FGF21 decreases body weight without reducing food intake or bone mineral density in high-fat fed obese rhesus macaque monkeys. Int. J. Obes. *42*, 1151–1160. https://doi.org/10.1038/s41366-018-0080-7.

24. Talukdar, S., Zhou, Y., Li, D., Rossulek, M., Dong, J., Somayaji, V., Weng, Y., Clark, R., Lanba, A., Owen, B.M., et al. (2016). A Long-Acting FGF21 Molecule, PF-05231023, Decreases Body Weight and Improves Lipid Profile in Non-human Primates and Type 2 Diabetic Subjects. Cell Metab. *23*, 427–440. https://doi.org/10.1016/j.cmet.2016.02.001.

25. Gaich, G., Chien, J.Y., Fu, H., Glass, L.C., Deeg, M.A., Holland, W.L., Kharitonenkov, A., Bumol, T., Schilske, H.K., and Moller, D.E. (2013). The effects of LY2405319, an FGF21 analog, in obese human subjects with type 2 diabetes. Cell Metab. *18*, 333–340. https://doi.org/10.1016/j.cmet.2013.08.005.

26. Hondares, E., Rosell, M., Gonzalez, F.J., Giralt, M., Iglesias, R., and Villarroya, F. (2010). Hepatic FGF21 expression is induced at birth via PPARalpha in response to milk intake and contributes to thermogenic activation of neonatal brown fat. Cell Metab. *11*, 206–212. https://doi.org/10.1016/j.cmet.2010.02.001.

27. Laeger, T., Henagan, T.M., Albarado, D.C., Redman, L.M., Bray, G.A., Noland, R.C., Münzberg, H., Hutson, S.M., Gettys, T.W., Schwartz, M.W., et al. (2014). FGF21 is an endocrine signal of protein restriction. J. Clin. Investig. *124*, 3913–3922. https://doi.org/10.1172/jci74915.

28. von Holstein-Rathlou, S., BonDurant, L.D., Peltekian, L., Naber, M.C., Yin, T.C., Claflin, K.E., Urizar, A.I., Madsen, A.N., Ratner, C., Holst, B., et al. (2016). FGF21 Mediates Endocrine Control of Simple Sugar Intake and Sweet Taste Preference by the Liver. Cell Metab. *23*, 335–343. https://doi.org/10.1016/j.cmet.2015.12.003.

29. Claflin, K.E., Sullivan, A.I., Naber, M.C., Flippo, K.H., Morgan, D.A., Neff, T.J., Jensen-Cody, S.O., Zhu, Z., Zingman, L.V., Rahmouni, K., et al. (2022). Pharmacological FGF21 signals to glutamatergic neurons to enhance leptin action and lower body weight during obesity. Mol. Metab. *64*, 101564. https://doi.org/10.1016/j.molmet.2022.101564.

30. Owen, B.M., Ding, X., Morgan, D.A., Coate, K.C., Bookout, A.L., Rahmouni, K., Kliewer, S.A., and Mangelsdorf, D.J. (2014). FGF21 acts centrally to induce sympathetic nerve activity, energy expenditure, and weight loss. Cell Metab. *20*, 670–677. https://doi.org/10.1016/j.cmet.2014.07.012.

31. Jensen-Cody, S.O., Flippo, K.H., Claflin, K.E., Yavuz, Y., Sapouckey, S.A., Walters, G.C., Usachev, Y.M., Atasoy, D., Gillum, M.P., and Potthoff, M.J. (2020). FGF21 Signals to Glutamatergic Neurons in the Ventromedial Hypothalamus to Suppress Carbohydrate Intake. Cell Metab. *32*, 273–286.e6. https://doi.org/10.1016/j.cmet.2020.06.008.

32. Rui, L. (2013). Brain regulation of energy balance and body weight. Rev. Endocr. Metab. Disord. *14*, 387–407. https://doi.org/10.1007/s11154-013-9261-9.

33. Cheng, W., Gordian, D., Ludwig, M.Q., Pers, T.H., Seeley, R.J., and Myers, M.G., Jr. (2022). Hindbrain circuits in the control of eating behaviour and energy balance. Nat. Metab. *4*, 826–835. https://doi.org/10.1038/s42255-022-00606-9.

34. Roman, C.W., Derkach, V.A., and Palmiter, R.D. (2016). Genetically and functionally defined NTS to PBN brain circuits mediating anorexia. Nat. Commun. *7*, 11905. https://doi.org/10.1038/ncomms11905.

35. Cheng, W., Gonzalez, I., Pan, W., Tsang, A.H., Adams, J., Ndoka, E., Gordian, D., Khoury, B., Roelofs, K., Evers, S.S., et al. (2020). Calcitonin Receptor Neurons in the Mouse Nucleus Tractus Solitarius Control Energy Balance via the Non-aversive Suppression of Feeding. Cell Metab. *31*, 301–312.e5. https://doi.org/10.1016/j.cmet.2019.12.012.

36. Cheng, W., Ndoka, E., Maung, J.N., Pan, W., Rupp, A.C., Rhodes, C.J., Olson, D.P., and Myers, M.G., Jr. (2021). NTS Prlh overcomes orexigenic stimuli and ameliorates dietary and genetic forms of obesity. Nat. Commun. *12*, 5175. https://doi.org/10.1038/s41467-021-25525-3.

37. Ludwig, M.Q., Cheng, W., Gordian, D., Lee, J., Paulsen, S.J., Hansen, S.N., Egerod, K.L., Barkholt, P., Rhodes, C.J., Secher, A., et al. (2021). A genetic map of the mouse dorsal vagal complex and its role in obesity. Nat. Metab. *3*, 530–545. https://doi.org/10.1038/s42255-021-00363-1.

38. Hayes, M.R., Leichner, T.M., Zhao, S., Lee, G.S., Chowansky, A., Zimmer, D., De Jonghe, B.C., Kanoski, S.E., Grill, H.J., and Bence, K.K. (2011). Intracellular signals mediating the food intake-suppressive effects of hindbrain glucagon-like peptide-1 receptor activation. Cell Metab. *13*, 320–330. https://doi.org/10.1016/j.cmet.2011.02.001.

39. Gabery, S., Salinas, C.G., Paulsen, S.J., Ahnfelt-Rønne, J., Alanentalo, T., Baquero, A.F., Buckley, S.T., Farkas, E., Fekete, C., Frederiksen, K.S., et al. (2020). Semaglutide lowers body weight in rodents via distributed neural pathways. JCI Insight *5*, e133429. https://doi.org/10.1172/jci.insight.133429.

40. Grill, H.J., and Hayes, M.R. (2012). Hindbrain neurons as an essential hub in the neuroanatomically distributed control of energy balance. Cell Metab. *16*, 296–309. https://doi.org/10.1016/j.cmet.2012.06.015.

41. Cao, W.H., Madden, C.J., and Morrison, S.F. (2010). Inhibition of brown adipose tissue thermogenesis by neurons in the ventrolateral medulla and in the nucleus tractus solitarius. Am. J. Physiol. Regul. Integr. Comp. Physiol. *299*, R277–R290. https://doi.org/10.1152/ajpregu.00039.2010.

42. Rogers, R.C., Barnes, M.J., and Hermann, G.E. (2009). Leptin "gates" thermogenic action of thyrotropin-releasing hormone in the hindbrain. Brain Res. *1295*, 135–141. https://doi.org/10.1016/j.brainres.2009.07.063.

43. Tran, L.T., Park, S., Kim, S.K., Lee, J.S., Kim, K.W., and Kwon, O. (2022). Hypothalamic control of energy expenditure and thermogenesis. Exp. Mol. Med. *54*, 358–369. https://doi.org/10.1038/s12276-022-00741-z.

44. Bruning, J.C., and Fenselau, H. (2023). Integrative neurocircuits that control metabolism and food intake. Science *381*, eabl7398. https://doi.org/10.1126/science.abl7398.

45. Xu, Q., Tam, M., and Anderson, S.A. (2008). Fate mapping Nkx2.1-lineage cells in the mouse telencephalon. J. Comp. Neurol. *506*, 16–29. https://doi.org/10.1002/cne.21529.

46. Ring, L.E., and Zeltser, L.M. (2010). Disruption of hypothalamic leptin signaling in mice leads to early-onset obesity, but physiological adaptations in mature animals stabilize adiposity levels. J. Clin. Investig. *120*, 2931–2941. https://doi.org/10.1172/JCI41985.

47. Claflin, K.E., Flippo, K.H., Sullivan, A.I., Naber, M.C., Zhou, B., Neff, T.J., Jensen-Cody, S.O., and Potthoff, M.J. (2022). Conditional gene targeting using UCP1-Cre mice directly targets the central nervous system beyond thermogenic adipose tissues. Mol. Metab. *55*, 101405. https://doi.org/10.1016/j.molmet.2021.101405.

48. Nakamura, K., Kimura, S., Yamazaki, M., Kawaguchi, A., Inoue, K., and Sakai, T. (2001). Immunohistochemical analyses of thyroid-specific enhancer-binding protein in the fetal and adult rat hypothalami and pituitary glands. Brain Res. Dev. Brain Res. *130*, 159–166. https://doi.org/10.1016/s0165-3806(01)00226-7.

49. Lee, B.J., Cho, G.J., Norgren, R.B., Jr., Junier, M.P., Hill, D.F., Tapia, V., Costa, M.E., and Ojeda, S.R. (2001). TTF-1, a homeodomain gene required for diencephalic morphogenesis, is postnatally expressed in the neuroendocrine brain in a developmentally regulated and cell-specific fashion. Mol. Cell. Neurosci. *17*, 107–126. https://doi.org/10.1006/mcne.2000.0933.

50. Flippo, K.H., Trammell, S.A.J., Gillum, M.P., Aklan, I., Perez, M.B., Yavuz, Y., Smith, N.K., Jensen-Cody, S.O., Zhou, B., Claflin, K.E., et al. (2022). FGF21 suppresses alcohol consumption through an amygdalo-striatal circuit. Cell Metab. *34*, 317–328.e6. https://doi.org/10.1016/j.cmet.2021.12.024.

51. Rose, J.P., Morgan, D.A., Sullivan, A.I., Fu, X., Inigo-Vollmer, M., Burgess, S.C., Meyerholz, D.K., Rahmouni, K., and Potthoff, M.J. (2025). FGF21 reverses MASH through coordinated actions on the CNS and liver. Cell Metab. *37*, 1515–1529.e6. https://doi.org/10.1016/j.cmet.2025.04.014.

52. Stanic, S., Bardova, K., Janovska, P., Rossmeisl, M., Kopecky, J., and Zouhar, P. (2024). Prolonged FGF21 treatment increases energy expenditure and induces weight loss in obese mice independently of UCP1 and adrenergic signaling. Biochem. Pharmacol. *221*, 116042. https://doi.org/10.1016/j.bcp.2024.116042.

53. Ferrari, L.L., Ogbeide-Latario, O.E., Gompf, H.S., and Anaclet, C. (2022). Validation of DREADD agonists and administration route in a murine model of sleep enhancement. J. Neurosci. Methods *380*, 109679. https://doi.org/10.1016/j.jneumeth.2022.109679.

54. Steculorum, S.M., Ruud, J., Karakasilioti, I., Backes, H., Engström Ruud, L., Timper, K., Hess, M.E., Tsaousidou, E., Mauer, J., Vogt, M.C., et al. (2016). AgRP Neurons Control Systemic Insulin Sensitivity via Myostatin Expression in Brown Adipose Tissue. Cell *165*, 125–138. https://doi.org/10.1016/j.cell.2016.02.044.

55. Claflin, K.E., Sullivan, A.I., Naber, M.C., Flippo, K.H., Morgan, D.A., Neff, T.J., Jensen-Cody, S.O., Zhu, Z., Zingman, L.V., Rahmouni, K., et al. (2022). Pharmacological FGF21 Signals to Glutamatergic Neurons to Enhance Leptin Action and Lower Body Weight During Obesity. Mol Metab. *64*, 101564.

56. Bruce, K., Garrido, A.N., Zhang, S.Y., and Lam, T.K.T. (2024). Regulation of Energy and Glucose Homeostasis by the Nucleus of the Solitary Tract and the Area Postrema. Endocrinol. Metab. *39*, 559–568. https://doi.org/10.3803/EnM.2024.2025.

57. Hermann, G.E., Barnes, M.J., and Rogers, R.C. (2006). Leptin and thyrotropin-releasing hormone: cooperative action in the hindbrain to activate brown adipose thermogenesis. Brain Res. *1117*, 118–124. https://doi.org/10.1016/j.brainres.2006.08.018.

58. Rogers, R.C., McDougal, D.H., and Hermann, G.E. (2011). Leptin amplifies the action of thyrotropin-releasing hormone in the solitary nucleus: an in vitro calcium imaging study. Brain Res. *1385*, 47–55. https://doi.org/10.1016/j.brainres.2011.02.029.

59. Scott, M.M., Williams, K.W., Rossi, J., Lee, C.E., and Elmquist, J.K. (2011). Leptin receptor expression in hindbrain Glp-1 neurons regulates food intake and energy balance in mice. J. Clin. Investig. *121*, 2413–2421. https://doi.org/10.1172/JCI43703.

60. Bookout, A.L., de Groot, M.H.M., Owen, B.M., Lee, S., Gautron, L., Lawrence, H.L., Ding, X., Elmquist, J.K., Takahashi, J.S., Mangelsdorf, D.J., et al. (2013). FGF21 regulates metabolism and circadian behavior by acting on the nervous system. Nat. Med. *19*, 1147–1152. https://doi.org/10.1038/nm.3249.

61. Dowsett, G.K.C., Lam, B.Y.H., Tadross, J.A., Cimino, I., Rimmington, D., Coll, A.P., Polex-Wolf, J., Knudsen, L.B., Pyke, C., and Yeo, G.S.H. (2021). A survey of the mouse hindbrain in the fed and fasted states using single-nucleus RNA sequencing. Mol. Metab. *53*, 101240. https://doi.org/10.1016/j.molmet.2021.101240.

62. Cheng, W., Ndoka, E., Hutch, C., Roelofs, K., MacKinnon, A., Khoury, B., Magrisso, J., Kim, K.S., Rhodes, C.J., Olson, D.P., et al. (2020). Leptin receptor-expressing nucleus tractus solitarius neurons suppress food intake independently of GLP1 in mice. JCI Insight *5*, e134359. https://doi.org/10.1172/jci.insight.134359.

63. Samms, R.J., Smith, D.P., Cheng, C.C., Antonellis, P.P., Perfield, J.W., 2nd, Kharitonenkov, A., Gimeno, R.E., and Adams, A.C. (2015). Discrete Aspects of FGF21 In Vivo Pharmacology Do Not Require UCP1. Cell Rep. *11*, 991–999. https://doi.org/10.1016/j.celrep.2015.04.046.

64. Veniant, M.M., Sivits, G., Helmering, J., Komorowski, R., Lee, J., Fan, W., Moyer, C., and Lloyd, D.J. (2015). Pharmacologic Effects of FGF21 Are Independent of the "Browning" of White Adipose Tissue. Cell Metab. *21*, 731–738. https://doi.org/10.1016/j.cmet.2015.04.019.

65. Klein Hazebroek, M., and Keipert, S. (2022). Obesity-resistance of UCP1-deficient mice associates with sustained FGF21 sensitivity in inguinal adipose tissue. Front. Endocrinol. *13*, 909621. https://doi.org/10.3389/fendo.2022.909621.

66. Chen, M.Z., Chang, J.C., Zavala-Solorio, J., Kates, L., Thai, M., Ogasawara, A., Bai, X., Flanagan, S., Nunez, V., Phamluong, K., et al. (2017). FGF21 mimetic antibody stimulates UCP1-independent brown fat thermogenesis via FGFR1/betaKlotho complex in non-adipocytes. Mol. Metab. *6*, 1454–1467. https://doi.org/10.1016/j.molmet.2017.09.003.

67. Liu, X., Rossmeisl, M., McClaine, J., Riachi, M., Harper, M.E., and Kozak, L.P. (2003). Paradoxical resistance to diet-induced obesity in UCP1-deficient mice. J. Clin. Investig. *111*, 399–407. https://doi.org/10.1172/JCI15737.

68. Bunk, J., Hussain, M.F., Delgado-Martin, M., Samborska, B., Ersin, M., Shaw, A., Rahbani, J.F., and Kazak, L. (2025). The Futile Creatine Cycle powers UCP1-independent thermogenesis in classical BAT. Nat. Commun. *16*, 3221. https://doi.org/10.1038/s41467-025-58294-4.

69. Holt, M.K. (2022). The ins and outs of the caudal nucleus of the solitary tract: An overview of cellular populations and anatomical connections. J. Neuroendocrinol. *34*, e13132. https://doi.org/10.1111/jne.13132.

70. Murphy, S., Collis Glynn, M., Dixon, T.N., Grill, H.J., McNally, G.P., and Ong, Z.Y. (2023). Nucleus of the solitary tract A2 neurons control feeding behaviors via projections to the paraventricular hypothalamus. Neuropsychopharmacology *48*, 351–361. https://doi.org/10.1038/s41386-022-01448-5.

71. Mota, C.M.D., and Madden, C.J. (2023). High Fat Diet Suppresses Energy Expenditure Via Neurons in the Brainstem. Neuroscience *520*, 84–94. https://doi.org/10.1016/j.neuroscience.2023.04.006.

72. Nakamura, K., and Morrison, S.F. (2010). A thermosensory pathway mediating heat-defense responses. Proc. Natl. Acad. Sci. USA *107*, 8848–8853. https://doi.org/10.1073/pnas.0913358107.

73. Bamshad, M., Song, C.K., and Bartness, T.J. (1999). CNS origins of the sympathetic nervous system outflow to brown adipose tissue. Am. J. Physiol. *276*, R1569–R1578. https://doi.org/10.1152/ajpregu.1999.276.6.R1569.

74. Doslikova, B., Tchir, D., McKinty, A., Zhu, X., Marks, D.L., Baracos, V.E., and Colmers, W.F. (2019). Convergent neuronal projections from paraventricular nucleus, parabrachial nucleus, and brainstem onto gastrocnemius muscle, white and brown adipose tissue in male rats. J. Comp. Neurol. *527*, 2826–2842. https://doi.org/10.1002/cne.24710.

75. Madden, C.J., and Morrison, S.F. (2009). Neurons in the paraventricular nucleus of the hypothalamus inhibit sympathetic outflow to brown adipose tissue. Am. J. Physiol. Regul. Integr. Comp. Physiol. *296*, R831–R843. https://doi.org/10.1152/ajpregu.91007.2008.

76. Nakamura, K., and Morrison, S.F. (2008). Preoptic mechanism for cold-defensive responses to skin cooling. J. Physiol. *586*, 2611–2620. https://doi.org/10.1113/jphysiol.2008.152686.

77. Yang, W.Z., Du, X., Zhang, W., Gao, C., Xie, H., Xiao, Y., Jia, X., Liu, J., Xu, J., Fu, X., et al. (2020). Parabrachial neuron types categorically encode thermoregulation variables during heat defense. Sci. Adv. *6*, eabb9414. https://doi.org/10.1126/sciadv.abb9414.

78. Yang, W.Z., Xie, H., Du, X., Zhou, Q., Xiao, Y., Zhao, Z., Jia, X., Xu, J., Zhang, W., Cai, S., et al. (2023). A parabrachial-hypothalamic parallel circuit governs cold defense in mice. Nat. Commun. *14*, 4924. https://doi.org/10.1038/s41467-023-40504-6.

79. Huang, K.P., Acosta, A.A., Ghidewon, M.Y., McKnight, A.D., Almeida, M.S., Nyema, N.T., Hanchak, N.D., Patel, N., Gbenou, Y.S.K., Adriaenssens, A.E., et al. (2024). Dissociable hindbrain GLP1R circuits for satiety and aversion. Nature *632*, 585–593. https://doi.org/10.1038/s41586-024-07685-6.

80. Gilroy, C.A., Capozzi, M.E., Varanko, A.K., Tong, J., D'Alessio, D.A., Campbell, J.E., and Chilkoti, A. (2020). Sustained release of a GLP-1 and FGF21 dual agonist from an injectable depot protects mice from obesity and hyperglycemia. Sci. Adv. *6*, eaaz9890. https://doi.org/10.1126/sciadv.aaz9890.

81. Muller, T.D., Sullivan, L.M., Habegger, K., Yi, C.X., Kabra, D., Grant, E., Ottaway, N., Krishna, R., Holland, J., Hembree, J., et al. (2012). Restoration of leptin responsiveness in diet-induced obese mice using an optimized leptin analog in combination with exendin-4 or FGF21. J. Pept. Sci. *18*, 383–393. https://doi.org/10.1002/psc.2408.

82. Ferraz Barbosa, B., Aquino de Moraes, F.C., Bordignon Barbosa, C., Palavicini Santos, P.T.K., Pereira da Silva, I., Araujo Alves da Silva, B., Cristine Marques Barros, J., Rodríguez Burbano, R.M., Pereira Carneiro Dos Santos, N., and Rodrigues Fernandes, M. (2023). Efficacy and Safety of Setmelanotide, a Melanocortin-4 Receptor Agonist, for Obese Patients: A Systematic Review and Meta-Analysis. J. Pers. Med. *13*, 1460. https://doi.org/10.3390/jpm13101460.

83. Qi, Y., Yu, T., Xu, J., Wan, P., Ma, Y., Zhu, J., Li, Y., Gong, H., Luo, Q., and Zhu, D. (2019). FDISCO: Advanced solvent-based clearing method for imaging whole organs. Sci. Adv. *5*, eaau8355. https://doi.org/10.1126/sciadv.aau8355.

84. Li, Y., Xu, J., Wan, P., Yu, T., and Zhu, D. (2018). Optimization of GFP Fluorescence Preservation by a Modified uDISCO Clearing Protocol. Front. Neuroanat. *12*, 67. https://doi.org/10.3389/fnana.2018.00067.

85. Pan, C., Cai, R., Quacquarelli, F.P., Ghasemigharagoz, A., Lourbopoulos, A., Matryba, P., Plesnila, N., Dichgans, M., Hellal, F., and Ertürk, A. (2016). Shrinkage-mediated imaging of entire organs and organisms using uDISCO. Nat. Methods *13*, 859–867. https://doi.org/10.1038/nmeth.3964.

86. Ting, J.T., Lee, B.R., Chong, P., Soler-Llavina, G., Cobbs, C., Koch, C., Zeng, H., and Lein, E. (2018). Preparation of Acute Brain Slices Using an Optimized N-Methyl-D-glucamine Protective Recovery Method. J. Vis. Exp. 53825. https://doi.org/10.3791/53825.

87. Banks, A.S., Allison, D.B., Alquier, T., Churchill, G.A., Ansarullah, Austad, S.N., Auwerx, J., Ayala, J.E., Baur, J.A., Carobbio, S., et al. (2025). A consensus guide to preclinical indirect calorimetry experiments. Nat. Metab. *7*, 1765–1780. https://doi.org/10.1038/s42255-025-01360-4.

STAR★METHODS

KEY RESOURCES TABLE

REAGENT or RESOURCE	SOURCE	IDENTIFIER
Antibodies		
HA-Tag (C29F4) Rabbit Monoclonal Antibody	Cell signaling	3724
c-Fos (9F6) Rabbit Monoclonal Antibody	Cell signaling	2250
Alexa Fluor™ 568 goat anti-rabbit IgG (H + L)	Invitrogen	3154584
Alexa Fluor™ 488 goat anti-rabbit IgG (H + L)	Invitrogen	3192622
Bacterial and virus strains		
AAV2/9CMVCreEGFP	University of Iowa viral vector core	N/A
AAV2/9CMVeGFP	University of Iowa viral vector core	N/A
AAV-hSyn-DIO-hM3Dq(Gq)-mCherry	Addgene	Cat# 44361-AAV2
AAV-hSyn-DIO-mCherry	Addgene	Cat# 50459-AAV2
AAV-hSyn-DIO-EGFP	Addgene	Cat# 50457-AAVrg
AAV-FLEX-tdTomato	Addgene	Cat# 28306
AAV-EF1a-Flpo	Addgene	Cat# 55637-AAVrg
AAV-EF1a-fDIO-Cre	Addgene	Cat# 121675-AAV9
Chemicals, peptides, and recombinant proteins		
Recombinant hFGF21	NovoNordisk	N/A
PF-05231023	Pfizer	N/A
CNQX	Tocris	Cat#: 0190
D-AP5	Tocris	Cat#: 0106
PTX	Tocris	Cat#: 1128
Deschloroclozapine dihydrochloride (DCZ) (water soluble)	Hello Bio	HB9126
Clozapine-N-oxide	Tocris	Cat#: 4936
Gill's Hematoxylin I	StatLab	SL97-16 PINT
Ammonium hydroxide solution	Sigma	320145
Critical commercial assays		
Fibroblast Growth Factor 21 Human ELISA	BioVendor	Cat#: RD191108200R
Ultra Sensitive Mouse Insulin ELISA	Crystal Chem	90080
Infinity Triglyceride	Infinity, Thermo Scientific	TR13421
Verichem Labs Matrix Plus Chemistry Reference Kit	Fisher Scientific	NC9592194
High-Capacity cDNA Reverse Transcription Kit	Life Technologies	4368814
SYBR green SYBR Greener QPCR for ABI 2000rxns	Thermofisher	1176002K
Autokit Glucose	Wako Diagnostics	439–90901
RNAscope 2.5 HD Detection Reagent -RED	Advanced Cell Diagnostics	322360
RNAscope H2O2 and Protease Reagents	Advanced Cell Diagnostics	322381
RNAscope Wash Buffer Reagents	Advanced Cell Diagnostics	310091
RNAscope Target Retrieval Reagents	Advanced Cell Diagnostics	322000
RNAscope Positive control probe Mm PPIB	Advanced Cell Diagnostics	313911
RNAscope Negative control probe Mm DapB	Advanced Cell Diagnostics	310043
RNAscope Probe - Mm-Klb-O1	Advanced Cell Diagnostics	481211

(*Continued on next page*)

Continued

REAGENT or RESOURCE	SOURCE	IDENTIFIER
Experimental models: Organisms/strains		
Nkx2.1-Cre	The Jackson Laboratory	008661
KLB$^{fl/fl}$	Ding et al.[18]	N/A
KLB loxTB	Flippo et al.[50]	N/A
KLB-Cre	Jensen-Cody et al.[31]	N/A
Vglut2-IRES-FLP	The Jackson Laboratory	030212
Ai65-tdTOMATO	The Jackson Laboratory	N/A
C57BL/6J	The Jackson Laboratory	003548
Oligonucleotides		
Primers for U36B4: 5′-CGTCCTCGTTGGAG TGACA-3′, 5’- CGGTGCGTCAGGGATTG-3’;	Jensen-Cody et al.[31]	N/A
Primers for Ucp1: 5’ - AAGCTGTGCGAT GTCCATGT-3’, 5’ -AAGCCACAAACCCT TTGAAAA-3′	Jensen-Cody et al.[31]	N/A
Primers for Bmp8b: 5’ - TCAACACAAC CCTCCACATCA-3’, 5’ -AGATCGGAGC GTCTGAAGATC-3′	Jensen-Cody et al.[31]	N/A
Software and algorithms		
GraphPad Prism 9	GraphPad	http://www.graphpad.com/scientific-software/prism/
Promethion Live	Sable Systems International	https://www.sablesys.com/products/promethion-core-line/promethion-live-software-platform/
Axon pCLAMP 11.2.2 software	Molecular Devices	N/A
Imaris	Oxford Instruments	N/A
PowerLab (for SNA recording)	ADInstruments	N/A
ImspectorPro	LaVision BioTec	N/A
Other		
Mouse chow diet	Teklad	2920X
60% HFD	Research Diets	D12492
ALZET osmotic pump	Alzet	1002
EcoMount	Biocare medical	EM897L
VECTASHIELD antifade mounting medium with DAPI	Vector Laboratories	H-1200-10
Trizol	Invitrogen	15596026

EXPERIMENTAL MODEL AND STUDY PARTICIPANT DETAILS

Animals

The following mice were utilized in these studies: Nkx2.1-Cre (JAX 008661), KLB$^{fl/fl}$,[18] KLB loxTB,[50] KLB-Cre; Vglut2-flp-Ai65,[29] and KLB-Cre.[31] All mice used in experiments were males on a C57BL/6J genetic background, except for KLB loxTB male mice which were on a mixed background (C57BL6/129Sv). The age of mice for each experiment is indicated in the figure legends. Mice were individually housed in a 12 h light/dark cycle at 22°C–23°C. Mice were given *ad libitum* access to chow (Teklad; 2920X) or 60% HFD (Research Diets; D12492). Health status was normal for all animals. All experiments presented in this study were conducted according to the animal research guidelines from NIH and were approved by the University of Iowa IACUC or the University of Oklahoma Health Sciences Center IACUC.

METHOD DETAILS

Administration of recombinant FGF21

16–20-week-old DIO $KLB^{Nkx2.1-Cre}$, KLB loxTB, $KLB^{fl/fl}$ and control littermates on 60% HFD for 8 weeks were randomized by body weight to receive either vehicle or FGF21 (1 mg/kg/day) via minipump (ALZET, 1002). Mice were individually housed for 2–5 weeks prior to surgery. Mice were then subcutaneously implanted with osmotic minipumps, and body weight was recorded daily for 2 weeks.

Administration of PF-05231023

16–18-week-old DIO WT and $KLB^{Nkx2.1-Cre}$ mice on 60% HFD for 8 weeks were randomized by body weight to receive either vehicle or PF-05231023. Mice were given an intraperitoneal (i.p.) injection of vehicle or PF-05231023 (3 mg/kg) every three days and body weight was recorded with every injection.

Surgery

Adult mice (8–18 weeks old) were anesthetized with 2%–3% isoflurane and placed on a stereotaxic frame. Heat pads were used through the duration of the surgery to keep the body temperature stable. Eye ointment was applied to keep the eyes from drying. An incision was made to the skin to expose the skull after asepsis with Betadine and medical alcohol application. For viral injection, a craniotomy was made and a 10 μL Hamilton syringe was slowly inserted with an injection speed of 100 nL per minute. The following coordinates were used for injection into the listed brain regions: hypothalamus (AP -1.34, ML ±0.5, DV -5.8 to −4.8), nucleus of the solitary tract (NTS, AP -7, ML ±0.5, DV -5.1 and −4.9), paraventricular nucleus (PVN, AP -0.8, ML ±0.35, DV -4.8), parabrachial nucleus (PBN, AP -5.05, ML ±1.4, DV -3.8). To facilitate viral spread across the hypothalamus, a large volume (1 μL) of AAV was injected as the syringe continuously moved up across the ventral-dorsal span (1mm) of the hypothalamus throughout viral infusion. Animals recovered for at least 4 weeks after surgery to allow for viral expression.

Whole organ clearing

An augmented DISCO protocol[83,84] was utilized to clear whole brain tissue as previously described.[47] Mice were anesthetized and transcardially perfused with pH 9.5 saline followed by pH 9.5 4% PFA. After post-fixing in PFA overnight, the brains were washed 3 times in saline and dehydrated with 50% tetrahydrofuran (THF) in dH2O for 24 h. Every 24 h the brains were transferred to a higher concentration of THF (50%, 70%, 80%), all at pH = 9.5. Brains were incubated in 100% THF for 48 h, and the solution was replaced every 12 h to maximize tissue THF concentration. After the final incubation in 100% THF, brains were transferred to dichloromethane (DCM) for 3 h followed by BABB-D15 for 4 h.[85] All steps were performed at 4°C in the dark. Additionally, after transferring brains to a new solution, argon gas was flowed over the sample to minimize oxygen interaction with the sample. Cleared brains were imaged in BABB-D15 using a light sheet fluorescence microscope (LaVision BioTec Ultramicroscope II) interfaced with an Andor *Neo* sCMOS camera, an Olympus MVX10 zoom microscope body, and an MVPLAPO 2x dipping cap. Whole brain three-dimensional images were achieved using a 3x3 mosaic tile scan of a 2x optical zoom and a z stack with step size of 2.5 mm. The raw lossless TIFF files of the collected tile scans were stitched using the ImspectorPro software and reconstructed into three dimensions with Imaris File Converter. Images and movies of brain samples were captured with Imaris and edited in Shotcut.

AAV viral constructs

The following viral constructs were used in this study: AAV2/9CMVCreEGFP (University of Iowa viral vector core), AAV2/9CMVeGFP (University of Iowa viral vector core), AAV-hSyn-DIO-hM3D(Gq)-mCherry (Addgene # 44361-AAV2), AAV-hSyn-DIO-mCherry (Addgene # 50459-AAV2), AAV-hSyn-DIO-EGFP (Addgene # 50457-AAVrg), AAV-FLEX-tdTomato (Addgene #28306), AAV-EF1a-Flpo (Addgene # 55637-AAVrg), AAV-EF1a-fDIO-Cre (Addgene # 121675-AAV9). AAV-EF1a-fDIO-Cre was diluted 1:10 with 1X PBS.

Gene expression

Gene expression analyses were performed as described previously.[55] Briefly, RNA was isolated from the indicated tissues following Trizol (Invitrogen) protocol. 2 μg RNA from each sample was used to generate cDNA (High-Capacity cDNA Reverse Transcription Kit; Life Technologies), and QPCR was conducted using SYBR green (Invitrogen). QPCR primer sequences are as follows: *U36B4:* 5′-CGTCCTCGTTGGAGTGACA-3′, 5’- CGGTGCGTCAGGGATTG-3’; *Ucp1:* 5’ - AAGCTGTGCGATGTCCATGT-3’, 5’ -AAGCCAC AAACCCTTTGAAAA-3’*; Bmp8b:* 5’ - TCAACACAACCCTCCACATCA-3’, 5’ -AGATCGGAGCGTCTGAAGATC-3’.

Electrophysiology

For patch clamp recordings, Klb-CreVGlut2-flpAi65 tdTomato triple transgenic male mice were maintained on chow or HFD for 12 weeks. Brain sections containing the nucleus of the solitary tract (NTS) were prepared based on a previously published protocol.[86] Brains were enucleated from deeply anesthetized mice and placed in a slightly frozen NMDG-HEPES aCSF cutting solution (in mM): 92 NMDG, 2.5 KCl, 1.25 NaH_2PO_4, 30 $NaHCO_3$, 20 HEPES, 25 Glucose, 5 Na-Ascorbate, 2 Thiourea, 3 Na-Pyruvate, 10 $MgSO_4 \cdot 7H_2O$, and 0.5 $CaCl_2 \cdot 2H_2O$ (pH 7.3–7.4 with HCl; 300–310 mOsm). The cold solution was aerated with 95% O_2/5% CO_2, and 300 μm thick NTS slices were obtained with a vibratome. Obtained slices were transferred to the NMDG-HEPES aCSF solution

heated to 37°C. NaCl concentration was gradually brought to 50 μM over the course of 10 min. Slices were transferred to a 95% O_2/5% CO_2 aerated holding solution at room temperature (25°C) containing (in mM): 92 NaCl, 2.5 KCl, 1.2 NaH_2PO_4, 30 $NaHCO_3$, 20 HEPES, 25 Glucose, 5 Na-Ascorbate, 2 Thiourea, 3 Na-Pyruvate, 2 $MgSO_4 \cdot 7H_2O$, and 2 $CaCl_2 \cdot 2H_2O$ (pH 7.3–7.4; 300–310 mOsm). After NTS slices were incubated in the holding solution for at least 45 min, they were placed in the patch clamp recording chamber perfused with an aCSF solution containing (in mM): 124 NaCl, 2.5 KCl, 1.2 NaH_2PO_4, 24 $NaHCO_3$, 5 HEPES, 12.5 Glucose, 2 $MgSO_4 \cdot 7H_2O$, and 2 $CaCl_2 \cdot 2H_2O$ (pH 7.3–7.4; 300–310 mOsm). Fluorescence-guided loose seal recordings were performed in the presence of synaptic blockers (10 μM CNQX, 50 μM AP5, and 50 μM PTX). Firing frequency was measured before and after bath application of FGF21 (50ng/μL). MultiClamp 700B Amplifier (Molecular Devices, San Jose, CA) and Axon pCLAMP 11.2.2 software (Molecular Devices, San Jose, CA) were used to collect and analyze data.

RNAscope *in situ* hybridization

RNAscope chromogenic *in situ* hybridization was performed using the RNAscope 2.5 HD Red Assay (Advanced Cell Diagnostics). Fixed-frozen brain sections (20 μm) were mounted onto Superfrost Plus slides (Fisherbrand), air dried, and post-fixed in 4% paraformaldehyde at 4°C for 15 min. Following serial dehydration in ethanol, target retrieval was performed for 5 min on a steamer and the sections was treated with RNAscope Protease Plus for 12 min at 40°C. Target probe (Mm-KLB-O1) hybridization, signal amplification, and detection was performed according to the manufacturer's instructions. Sections were counterstained with hematoxylin, baked dry, and coversplipped with EcoMount. Images were acquired using an Olympus VS1200 microscope.

Immunohistochemistry

For immunohistochemistry, brains were collected and post-fixed for 24 h in 4% PFA and transferred to 30% sucrose for at least 48 h. Brains were cryoprotected in Tissue-Tek optimal cooling temperature (OCT) compound and stored at −80°C until use. 40 μm coronal sections were cut using a Leica cryostat. Brain sections were washed and incubated in blocking solution (5% goat serum in PBST (0.3% Triton X-100 in PBS)) for 1 h at room temperature. For immunohistochemical detection of the HA tag, slices were incubated in rabbit α-HA-tag (1:1000, Cell signaling # 3724) overnight at 4°C. The following day slices were washed and incubated with AlexaFluor568-fluorescently-conjuagted goat anti-rabbit secondary (1:1000, Life Technologies) for 2 h at room temperature. Following a wash, all sections were mounted with VECTASHIELD antifade mounting media with DAPI (Vector Laboratories # H-1200-10) and imaged using the Olympus VS200 slide scanner. For detection of c-fos, slices were incubated in rabbit anti c-fos (1:1000, Cell signaling # 2250) overnight at 4°C and with AlexaFluor488-fluorescently-conjugated goat anti-rabbit secondary (1:1000, Life Technologies #3192622) for 2 h at room temperature. The sections for c-fos detection was mounted with Prolong Gold antifade mounting media with DAPI (Invitrogen #P36930) and imaged using a Olympus VS120 slide scanner.

Indirect calorimetry

DIO WT and $KLB^{fl/fl}$ mice were individually housed in the Promethion Metabolic System (Sable Systems International) at the University of Iowa Metabolic Phenotyping Core on a 12 h light-dark cycle with *ad libitum* access to water and food at 23°C. Mice were housed in the Promethion for 5 days to record baseline measurements, removed and implanted with minipumps containing vehicle or FGF21. Following 7 days in home cages, mice were returned to Promethion housing for the last 5 days of FGF21 administration. Data was analyzed as previously described.[29] Importantly, we present energy expenditure data in absolute terms and interprer them alongside unchanged food intake and the observed thermogenic gene responses, rather than normalizing by body mass/lean mass. As emphasized by the recent guidelines for analysis of preclinical indirect calorimetry, simple ratio-based normalization (for example, expressing EE as EE/lean mass) can be misleading, particularly in models with altered adiposity.[87]

DIO KLB-Cre mice administered AAV-DIO-hM3Dq or AAV-DIO-mCherry were individually housed in the Promethion Metabolic System (Sable Systems International) at the University of Oklahoma Health Science Center on a 12 h light-dark cycle with *ad libitum* access to water and food at 23°C. Mice were housed in the Promethion for 5 days for habituation (day 1–3) and baseline measurements (day 4–5). Next, mice were administered DC in drinking water (2 mg/L) for two days. On the third day, DCZ was administered i.p. (1 mg/kg) at 10 a.m. and response in energy expenditure were analyzed for another 6 h.

Home cage food intake

Food intake was measured in home cages by weighing the weight of the food plus the food hopper daily. Mice that chewed food without consuming it resulting in very small pieces of food left on the cage floor were eliminated from food intake data.

Sympathetic nerve recordings

BAT sympathetic nerve activity was recorded under anesthesia as previously described.[30] Briefly, animals were anesthetized and instrumented with a colonic temperature probe. Cannulae were implanted into the common carotid artery and jugular vein. A sympathetic nerve subserving the BAT was isolated and suspended on 36-gauge platinum-iridium electrodes and secured with silicone gel. Electrodes were interfaced to a high-impedance probe (HIP-511; Grass Instruments), and the neural signal from BAT was amplified 100,000 times, filtered at low- and high-frequency cutoffs at 100 and 1,000 Hz, respectively, and routed to a resetting voltage integrator (B600c; University of Iowa Bioengineering). After a baseline reading was established, vehicle or FGF21 (1 μg/g body weight) was administered intravenously with the first half of the dose given in bolus, and the second half infused over the first 30 min. For

chemogenetic activation, vehicle or clozapine-N-oxide (CNO; 2 mg/kg) was administered intravenously as one bolus following baseline recording. Data was recorded using an ADInstruments PowerLab with the associated Chart software.

Plasma analyses

Blood was collected from fed mice in the morning into 300K2E microvettes (Sarstedt) and spun at 3000 rpm for 30 min at 4°C to separate plasma. Human FGF21 (Biovender) and mouse insulin (Crystal Chem Inc) were measured using commercially available ELISAs. Plasma glucose (Wako Diagnostics) was measured using colorimetric assays. All measurements were performed according to the manufacturer's instructions.

Hepatic lipid measurement

Hepatic triglyceride levels were quantified using the Folch method as previously described.[51] Livers were harvested, snap-frozen in liquid nitrogen, pulverized, and stored at −80°C until use. Briefly, 100–200 mg of tissue was homogenized in 2:1 v/v chloroform/methanol solution and allowed to sit at room temperature for approximately 30 minutes. 1 mL of 50 mM NaCl solution was added to each sample, vortexed, and centrifuged at 1000g for 10 min at room temperature. The organic phase was collected into a new tube and 1 mL of 0.36M CaCl2 in 1:1 v/v Methanol/H2O was added. The sample was then vortexed and centrifuged at 1000g for 10 min at room temperature. The organic phase was collected into a 5 mL glass volumetric flask and brought to a volume of 5 mL with fresh chloroform. Flasks were capped and the content sat at room temperature overnight before replacing residue water with fresh chloroform. All steps were performed using glass equipment. Triglycerides were quantified using commercially available kits (Infinity Triglycerides, Thermo Scientific) and standards (Matrix Plus Chemistry Reference Kit, Verichem) according to manufacturer's instructions.

QUANTIFICATION AND STATISTICAL ANALYSIS

Statistical analysis

Data were analyzed using GraphPadPrism and presented as mean ± SEM; $p < 0.05$ was considered significant. The statistical test used for each comparison is described in the corresponding figure legends.